



Brandenburg
University of Technology
Cottbus

Chair of Environmental Informatics
Environmental and Resource Management (B.Sc.)

Bachelor Thesis

A 2-D Numerical Hydrodynamic Flood Model of a Section of
the River Rhine and the Polder Mehrum

Supervisors:

apl. Prof. Dr.-Ing. habil. Frank Molkenhain
Chi-Yu Li

By:

Julian Wahl
Matr. Number: 2831968
Date of Birth: 01.05.1987
E-Mail: juliwahl@googlemail.com

Cottbus, July 29th, 2012

Declaration:

I declare that I have written this bachelor thesis myself and have not used other sources than the ones listed and made all information adapted from external sources recognizable as such. This work, in its complete form or parts of it, has not been submitted to any examination body before.

Cottbus, July 29th, 2012

Julian Wahl

Place, Date

Signature

Acknowledgements

I would like to express my sincere gratitude to my academic supervisor Prof. Frank Molkenhain who provided me with continuous support from the very beginning. His guidance greatly helped me in completing the work presented in this thesis. Furthermore, I would like to thank Chi-Yu Li and Vikram Notay, who always had an open ear for my questions and assisted me with their knowledge and insight.

Abstract:

Flood events frequently result in catastrophic losses of human life and properties. Numerical models can be used to predict the hydrodynamic characteristics of such incidents, and they can thereby greatly support the development of flood risk management strategies. The visualization and analysis of results from flood-inundation models can be enhanced through the integration of GIS systems, which can be used for the creation of detailed flood risk maps.

Subject of this thesis is the development of a 2-D model of a section of the river Rhine, and a simulation of a flooding of the polder Mehrum due to a dike failure. The model was created with the software package MIKE 21 Flow Model FM, which solves the shallow water equations on an unstructured grid by using a finite volume approach. Pre- and post-processing of the data was conducted in ArcGIS. The thesis presents some approaches of how GIS-systems can be used for the optimization of computational grids as well as for an improved visualization and analysis of simulation results.

The focus of the work was on the development of a computational grid for both the river and the polder which sufficiently describes the topography of the study area for the purpose of investigating the inundation processes. This included the determination of appropriate domain boundaries and the identification of an adequate number and distribution of computational nodes. For the river model furthermore, a calibration of the roughness coefficient was carried out to achieve an acceptable agreement with the observed data. A relatively large influence of the coefficient on calculated water levels was observed, from which it was concluded that the optimization of the parameter is indispensable for realistic results of hydrodynamic flood models. A further essential aspect was to represent the dike separating the river from the polder as a continuous linear feature so as to prevent inflow into the polder during non-breaching conditions. The polder inundation was simulated by making the simplified assumption of a complete collapse of a section of the dike. The simulated event is based on measured data which were obtained during the flood of January/February 1995. Temporal development of the inundation was visualized in ArcGIS by creating TINs representing water depths within the polder at characteristic time steps. Overlaying of these TINs onto different maps allowed then for the identification of affected areas.

Table of Contents

Declaration:.....	i
Acknowledgements.....	ii
Abstract:.....	iii
List of Figures.....	viii
List of Tables.....	xi
Abbreviations:.....	xii
1. Introduction.....	1
2. Numerical Hydrodynamic Models.....	2
2.1 3-D NHMs.....	3
2.2 1-D NHMs.....	3
2.2 2-D NHMs.....	4
2.3 Shallow Water-Equations.....	5
2.4 Roughness Coefficient.....	8
3. The Numerical Solution.....	9
3.1 Grid Generation.....	10
3.1.1 Structured Grids.....	10
3.1.2 Unstructured Grid:.....	10
3.2 The Finite Difference Method.....	11
3.3 The Finite Element Method.....	11
3.4 The Finite Volume Method.....	11
4. Topographic Data for NHMs.....	12
4.1 Methods for Data Collection.....	12
4.1.1 Photogrammetry.....	13
4.1.2 Light Detection and Ranging.....	13
4.1.3 Field Surveying Methods.....	14
4.1.4 Echo Sounding.....	14

4.1.5 Laser Bathymetry	15
4.2 Data Formats for the Representation of Surfaces.....	15
4.2.1 Raster based DEMs	16
4.2.2 Triangular Irregular Networks.....	16
5. The Applied Modeling Tools	17
5.1 Mike 21 Flow Model FM.....	17
5.1.1 Boundary Conditions.....	18
5.1.2 Initial Conditions	20
5.2 Mike Zero Mesh Generator.....	20
6. The Case Study	21
6.1 The Study Area.....	21
6.2 The Simulated Flood Event.....	24
6.3 Available Topographic Data	24
7. Creation of the Numerical Hydrodynamic Model	26
7.1 The Grid Generation.....	27
7.2 Definition of the Computational Domain.....	27
7.2.1 Upstream boundary.....	29
7.2.2 Downstream boundary.....	30
7.2.3 Representation of the Dike	31
7.3 Mesh Resolution.....	32
8. Set up of the Simulation File	35
8.1 Time Specification	35
8.2 Solution Technique	35
8.3 Density	36
8.4 Eddy viscosity	36
8.5 Roughness Coefficient	36
8.6 Specification of the Boundary Conditions	37

8.7 Initial Conditions.....	40
9. Hydraulic Performance for different Mesh Resolutions	41
9.1 Results	41
9.1.1 Discharge at Wesel	41
9.1.2 Water levels at Ruhrort.....	43
9.2 Discussion and Conclusion	45
10. Measures to Improve the Grid	46
10.1 Creation of an Internal Polygon for the River Channel.....	46
10.2 Creation of the Thalweg	47
10.3 Results of the Mesh Improvements	48
10.4 Conclusion.....	49
11. Calibration.....	49
11.1 Theoretical Background	49
11.2 Calibration of the Roughness Coefficient	50
11.3 Results	51
11.4 Discussion and Conclusion	52
12. Generation of the Polder Model.....	53
12.1 Introduction to the Modeling Task.....	53
12.2 Available Data.....	53
12.3 Creation of the Polder Boundary.....	54
12.4 Extraction of 3-D Points from the Polder Area.....	55
12.5 Determination of a Suitable Mesh Resolution for the Polder	55
12.5.1 Volumetric Comparison	55
12.5.2 The ArcGIS Tool “Decimate TIN Nodes”	59
13. The Combined Model	60
13.1 Dike Breach.....	61
13.2 Results	61

14. Visualization of the Results in ArcGIS.....	62
14.2 Discussion	64
15. Conclusion	65
16. Possible Future Steps	66
17. References.....	67
Appendix:.....	71

List of Figures

Figure 1: 1995 flood event, discharge at Ruhort.....	24
Figure 2: Available topographic data on a satellite image.....	25
Figure 3: Inundation areas for HQ500 with dikes and without dikes.....	26
Figure 4: Domain boundary points located at the outer extend of inundation areas for non-breaching conditions	28
Figure 5: Location of the upstream gauge in Ruhrort.....	29
Figure 6: The upstream boundary created along the measured data close to the stream gauge in Ruhrort.....	30
Figure 7: Upstream boundary created at river km 814 along the measured data Geoserver ..	30
Figure 8: Complete boundary of the computational domain on a satellite image and a flood inundation map.....	31
Figure 9: Representation of the dike separating the polder Mehrum from the river before a manual correction of the z-values was performed	32
Figure 10: Creation of TINs from mesh nodes generated in the MZMG	33
Figure 11: Diagram of the surface volume enclosed by TINs versus the number of nodes used to create these TINs, compared to the benchmark TIN.....	34
Figure 12: Pegel Ruhrort.....	38
Figure 13: Specified Q at the upstream boundry in Ruhrort.....	39
Figure 14: Specified water levels at the downstream boundary in Wesel	39
Figure 15: Spatially varying water levels used as initial conditions.....	40
Figure 16: Measured and calculated hydrographs at Wesel and corresponding relative percentage error for 2,000 and 16,000 nodes.....	42

Figure 17: Comparison of the observed and calculated water levels at Ruhrort for different mesh resolutions.....	44
Figure 18: Comparison of the relative errors in matching the observed water levels for different mesh resolutions.....	44
Figure 19: Internal polygon for the river channel.....	46
Figure 20: Internal polygon on a map showing the main river channel	47
Figure 21: Mesh with (left) and without the created thalweg feature.....	48
Figure 22: Comparison of the relative error (%) in the calculation of water levels for different meshes.....	49
Figure 23: Relative percentage error in the calculation of water levels for different Manning values	52
Figure 24: The created polder boundary on a flood inundation map for a scenario without dikes	54
Figure 25: Benchmark TIN of the polder area incorporating to complete available topographic information.....	56
Figure 26: Calculated volumes enclosed by TINs created from nodes which were extracted from meshes of increasing resolution, compared to the volume of a benchmark TIN containing the complete set of available topographic information.....	57
Figure 27: Absolute and relative errors of different mesh resolutions in matching the benchmark volume. The green dot represents a mesh of 4,000 nodes including significant topographic points extracted through the VIP method.	57
Figure 28: Reduced set of the Very Important Points (VIP) on the DEM.....	58
Figure 29: Combined model of the river and the polder including the specified initial water levels	60
Figure 30: Created dike breach from a perspective of the opposite river bank.....	61

Figure 31: Dike breach induced inflow (instantaneous and accumulated) into the polder.....	62
Figure 32: Temporal development of the inundation: Water depth within the polder at different time steps on a road map together with polygons for residential areas	64
Figure 33: Available topographic data on a river map	71
Figure 34: Model boundary at the upper section of the river	72
Figure 35: Mesh of the polder and the river channel	72
Figure 36: Boundary along the dike separating the polder Mehrum from the river	73
Figure 37: Initial Conditions	73
Figure 38: Specified Manning values	74
Figure 39: Maximum inundation of the polder	74
Figure 40: Mesh containing quadrangular elements for the main channel	75

List of Tables

Table 1: Symbol explanation of the above given equations	7
Table 2: Comparison of the volume enclosed by TINs with respect to the number of nodes used to create these TINs	34
Table 3: Information about the stream gauges in Wesel and Ruhrort	38
Table 4: AARE (%) for discharge, PEP and the required computational time for different mesh resolutions.....	43
Table 5: AARE and the absolute error range in the prediction of water levels as well as the required computational time for different mesh resolutions.....	45
Table 6: Absolute average relative error (AAER) for discharge (q) and water levels (h) and the required computational time for different meshes	48
Table 7: Absolute average relative error (AARE) and maximum relative error (max. RE) of different Manning coefficients (M) for discharge (q) and water levels (h)	51
Table 8: Number of nodes for different vertical accuracies	59

Abbreviations:

ALB:	Airborne Laser Bathymetry
ALIDAR:	Airborne Light Detection and Ranging
CFD:	Computational fluid dynamics
CFL:	Courant-Fridrichs-Lewy
DEM:	Digital Elevation Model
FDM:	Finite Difference Method
FEM:	Finite Element Method
FVM:	Finite Volume Method
M21fm:	Mike 21 Flow Model FM
MZMG:	Mike Zero Mesh Generator
NHMs:	Numerical Hydrodynamic Models
SWEs:	Shallow water equations

1. Introduction

All over the world flood events are becoming increasingly frequent and severe as a result of population growth, developmental activities on floodplains, deforestation and the effects of climate change (Zhang and Wu 2011). Dams and dikes are typical structural flood protection measures. However, river sections embanked by dikes can have a high damage potential. This is because areas protected by dikes are usually areas where intensive settlement and development activities occur. Furthermore, flow velocities from a dike breach outflow are usually high and can result in a rapid rise of water levels within the embanked areas leaving only limited time for the affected population to react (Vorogushyn 2008). To reduce the damages induced by dike failures to a minimum, emergency measures such as evacuation plans or early warning systems should be set up. For the proper development and implementation of these measures, information about the potential intensity of the inundation, the affected areas and the corresponding timing should be available. This information can be obtained through physical experiments or numerical simulations. The latter have become increasingly used and efficient due to the increases in the power of computers (Kao and Chang 2012). In fact, numerical flood inundation models have become central tools in the assessment of flood risk as well as in the real-time forecasting of floods (Pappenberger et al. 2006). They provide valuable decision support for the planning and maintenance of protective structures, the establishment of emergency and insurance measures and the implementation of floodplain development regulations. In addition to the assessment of flood risks, validated numerical hydrodynamic models (NHMs) of river channels and floodplains can also be used for investigations of sediment – or pollution transport processes (Horritt and Bates 2001).

Major tasks of flood risk assessment include the prediction of inundation extents, flood timings and flood intensity indicators such as water depths and flow velocities as well as an estimation of the associated damages. Flood risk maps are commonly used to visualize and communicate the results of such investigations. NHMs in combined use with GIS-systems can be used to create these maps. Furthermore, it is important to analyze the associated uncertainties of such models in order to allow decision makers to interpret the data correctly (Vorogushyn 2008). Initiatives of flood inundation mapping in Europe started to a larger extend in the late 1990s as a result of several major floods during that time. In 2007, the

European Union implemented a flood directive which puts all members states under the obligation to create flood risk maps and to develop flood risk management plans until 2015 (Cook and Merwade 2009).

In chapter 2 the theoretical background of NHMs will be provided. This includes a summary of models of different dimensionality, a description of the shallow water equations and information about the roughness coefficient. Chapter 3 deals with the numerical methods used to solve the governing equations of hydraulic models. Chapter 4 outlines aspects of the topographic data used in NHMs, gives an overview about different data collection methods, and analyses the most common data structures for storing topographic data for 2-D models. In chapter 5 the applied modeling tools namely Mike 21 Flow Model FM (M21fm) and the Mike Zero Mesh Generator (MZMG) will be described. Chapter 6 provides an introduction to the case study where the focus is on the study area, the simulated flood event and the available topographic data. In chapter 7 the main steps taken to create the computational grid are presented, including the definition of the domain boundaries and a volumetric analysis of the impact of mesh resolution on the model's representation of the topography. The setup of the simulation file is subject to chapter 8, where the specification of the model's main parameters is provided. Chapter 9 deals with the identification of an optimum mesh resolution for the river model. In chapter 10 two methods which were taken to improve the mesh are described and evaluated. Chapter 11 is devoted to the optimization of the roughness coefficient, including a presentation of the simulation results with different Manning values. Chapter 12 describes the process of generating the computational grid for the polder, i.e. the definition of the domain boundaries, extraction of topographic data from a DEM and a volumetric analysis of the mesh resolution in ArcGIS. In chapter 13 information about the final NHM including the created dike failure are given, and the simulation results for the breaching scenario are presented. The visualization of the inundation process in ArcGIS is subject to chapter 14. In chapter 15 final conclusions are drawn. Chapter 16 outlines potential future steps to improve the model.

2. Numerical Hydrodynamic Models

NHMs are based on the equations for the conservation of mass, momentum and energy. These equations are given in their general form by the Navier-Stokes equations, which are a system of non-linear partial differential equations. The complete three-dimensional equations

accurately describe even the most complex flows in detail, but their numerical solution requires that the entire range of spatial and temporal scales of the turbulence have to be resolved. Such a so called direct numerical simulation (DNS) is with the exception for very small computational areas and small Reynolds numbers computationally not feasible (Habersack et al. 2007). A first level of simplification can be achieved with so called large eddy simulations (LES) which eliminate smaller turbulences from the solution through a filtering process. Thus, only the larger eddies are resolved, while the small scale turbulences are parameterized (Wright and Crosato, 2011). Despite a considerable reduction of the computation costs, the required resolution for a LES is still too high to allow for an efficient simulation of flows in the natural environment. Thus, for the simulation of natural water bodies usually the Reynolds-averaged Navier-Stokes equations (RANS equations) are used. These are based on the decomposition of the dependent variables into time-averaged and fluctuating components (Malcherek 2012).

The complexity and thus the computational effort required for solving the initial Navier-Stokes equations can be further decreased by reducing the dimension of the equations. Generally one can distinguish between 3-D, 2-D and 1-D hydrodynamic models, where the dimension refers to the number of spatial dimensions for which flow variables are computed. The optimum type of model for a given case study should produce information at a detail sufficiently accurate for the intended investigation while staying within affordable computational costs and fitting the available data (Bates and De Roo 2000).

2.1 3-D NHMs

3-D hydrodynamic models solve the complete Navier Stokes equations. They thus result in high computational expenses. Furthermore, the model set up is complicated and time consuming. Hence, they are commonly only applied for very small domains where a detailed investigation of the flow is required. Application areas include hydrodynamic analysis at hydraulic structures (e.g. weirs, bridges or turbines) or the modeling of dam breaks (Habersack et al. 2007).

2.2 1-D NHMs

In 1-D NHMs flow velocities are averaged over the depth and the width of a river. This implies spatially constant water levels and flow velocities for a given river cross-section.

These assumptions are incorporated in the Saint Venant equations which are the governing equations of many commercial and non-commercial software packages such as MIKE 11, ISIS, or HEC-RAS. With these schemes, rivers are described as series of cross-sections for which—depending on the specified boundary conditions—the unknown flow variables are numerically computed. As the area between the cross-section is not explicitly accounted for, the selection of appropriate cross-sections is crucial for the accuracy of a 1-D model (Bates and De Roo 2000). A 1-D approach offers high computational efficiency, has relatively low data requirements and may be useful for comparatively straight rivers or river sections, where lateral and vertical velocities are low or not significant for the purpose of the study (Habersack et al. 2007; Wright and Crosato, 2011). However, there are several limitations of a 1-D hydrodynamic model including their inability to account for a detailed description of the river geometry. Due to these limitations, the use 1-D models for simulating flow in river channels has been increasingly replaced by 2-D models. This has particularly been stimulated by the increase in the speed of computers, which posed a significant constraint on the large scale application of 2-D models earlier (Merwade, et. al 2008).

Since flooding involves considerable lateral flow, potentially large differences between velocities in the main channel and on the inundated areas, and because flow paths on flooded areas are not known a priori, purely 1-D models are of limited suitability for investigations of flooding processes. However, to some degree it is possible with a 1-D model to determine inundation areas by intersecting a plane of interpolated water levels with a Digital Elevation Model (Bates and De Roo 2000). The disadvantage of this approach is that areas which are not hydraulically connected to the river might be identified as being flooded, and that an assessment of flow velocities is not possible (Vorogushyn 2008).

Another option is to couple a 1-D model describing the river channel with a 2-D model for the area to be flooded. Software package such as Mike Flood by DHI have been developed to allow for such an approach. However, according to Chua et al. such an approach is not suitable for rivers with strongly meandering patterns. In these cases an entirely 2-D approach should be preferred (Chua et. al 2001).

2.2 2-D NHMs

2-D hydrodynamic models compute the flow of fluids within a horizontal plane averaged over the depth of this plane. Hence, a 2-D model is able to simulate laterally varying flow

velocities and water levels within the domain. Furthermore, the flow path of the water body is not fixed but calculated by the model. These properties make a 2-D model particularly suitable for flood risk analysis. A disadvantage compared to 1-D models are the much longer computation times of a 2-D model. According to Habersack et al. (2007), the required computation time of a 2-D model is increased by a factor of 100 to 500 compared to a 1-D model.

A 2-D approach is selected for the investigation of the later presented case study as in terms of data availability, size of the computational area as well as due to the intention of simulating the inundation of the polder Mehrum it provides the most promising option. A 1-D model would not be able to represent the 2-D flooding process, and a 3-D approach would be unnecessary complex. However, according to Bates and De Roo (2000) the development of a strong shear layer at the channel-floodplain interface results in highly 3-D flows.

2-D NHMs are based on the shallow-water equations (SWEs) which will now be briefly described.

2.3 Shallow Water-Equations

The SWEs describe free surface hydrodynamics in vertically well-mixed water bodies. The SWEs are derived from the Navier-Stokes equations by integrating the horizontal velocity over the depth of the fluid. As a consequence, the intrinsically 3-D flow is simplified into a depth independent horizontal plane flow. That is, variables are averaged over the vertical direction, implying a uniform flow velocity with elevation. Thus, the vertical velocity of the fluid is removed from the equations, and only variables in x- and y- direction are approximated. The vertical integration is justified by the assumption that the horizontal length scale is much greater than the vertical length scale, and thus, changes in the variables with depth are insignificant in comparison to the changes in the horizontal directions. According to Tan (1992) the ratio of the vertical length scale to the horizontal length scale should be in the range of:

$$\frac{h}{L} < 10^{-3} \sim 10^{-4}$$

The SWE's is also based on the assumption of hydrostatic balance, i.e. the balance between the gravity and pressure gradient in the vertical direction. This assumption allows the

integration of the pressure over the water depth, and thereby allows replacing the unknown pressure by the water depth (David Randall 2006).

$$\frac{\partial p}{\partial z} = -\rho g$$

The density of the fluid is assumed to be vertically homogeneous, i.e. there is no stratification over the water elevation (DHI 2007):

$$\rho = \rho (x, y, t)$$

Furthermore, the SWEs are valid only for incompressible fluids, implying that the density of the fluid does not change during its motion. The independent variables of the SWEs are time, and the two coordinates for the horizontal plane. The dependent variables are the depth and the two-dimensional fluid velocity field. The main external force affecting the flow is gravity. Other forces may include the coriolis- and the tidal force, frictional forces at the water-land interface and wind forces exerted at the water surface (Wright and Crosato 2011).

The SWEs include one equation for the conservation of mass (i.e. the continuity equation) and two equations for the conservation of momentum. The differential formulation of these equations for a planar Cartesian co-ordinate system is given below (DHI 2007):

The local continuity equation:

$\frac{\partial h}{\partial t} + \frac{\partial h\bar{u}}{\partial x} + \frac{\partial h\bar{v}}{\partial y} = hS$	(1)
--	-----

The momentum equations for the x- and y component:

$\frac{\partial h\bar{u}}{\partial t} + \frac{\partial h\bar{u}^2}{\partial x} + \frac{\partial h\bar{v}\bar{u}}{\partial y} = f\bar{v}h - gh\frac{\partial \eta}{\partial x} - \frac{h}{\rho_0}\frac{\partial p_a}{\partial x} -$	(2)
$\frac{gh^2}{2\rho_0}\frac{\partial \rho}{\partial x} + \frac{\tau_{sx}}{\rho_0} - \frac{\tau_{bx}}{\rho_0} - \frac{1}{\rho_0}\left(\frac{\partial s_{xx}}{\partial x} + \frac{\partial s_{xy}}{\partial y}\right) +$	

$\frac{\partial}{\partial x}(hT_{xx}) + \frac{\partial}{\partial y}(hT_{xy}) + hu_s S$	
--	--

$\frac{\partial h\bar{v}}{\partial t} + \frac{\partial h\bar{u}\bar{v}}{\partial x} + \frac{\partial h\bar{v}^2}{\partial y} = f\bar{u}h - gh \frac{\partial \eta}{\partial y} - \frac{h}{\rho_0} \frac{\partial p_a}{\partial y} -$ $\frac{gh^2}{2\rho_0} \frac{\partial \rho}{\partial y} + \frac{\tau_{sy}}{\rho_0} - \frac{\tau_{by}}{\rho_0} - \frac{1}{\rho_0} \left(\frac{\partial s_{yx}}{\partial x} + \frac{\partial s_{yy}}{\partial y} \right) +$ $\frac{\partial}{\partial x}(hT_{xy}) + \frac{\partial}{\partial y}(hT_{yy}) + hv_s S$	(3)
---	-----

t : time	x, y, z : the Cartesian co-ordinates	η : surface elevation	$h = \eta + d$: the total water depth
u, v : the velocity components in the x and y direction	g : gravitational acceleration	ρ : the density of water ρ_0 : the reference density of water	$s_{xx}, s_{xy}, s_{yx}, s_{yy}$: components of the radiation stress tensor
$f = 2\Omega \sin \phi$: coriolis parameter	Ω : the angular rate of revolution ϕ : the geographic latitude	p_a : the atmospheric pressure	S : the magnitude of the discharge due to point sources u_s, v_s : the velocity by which the water is discharged into the ambient water

Table 1: Symbol explanation of the above given equations

The lateral stresses (T) include viscous friction, turbulent friction, and differential advection. They are predicted through an eddy viscosity formulation based on the depth average velocity gradients:

$T_{xx} = 2A \frac{\partial \bar{u}}{\partial x}$	$T_{xy} = A \left(\frac{\partial \bar{u}}{\partial y} + \frac{\partial \bar{v}}{\partial x} \right)$	$T_{yy} = 2A \frac{\partial \bar{v}}{\partial y}$	(4)
---	---	---	-----

The overbar indicates a depth averaged value. For example, \bar{u} and \bar{v} are the depth-averaged velocities defined as:

$h\bar{u} = \int_{-d}^n u dz,$	$h\bar{v} = \int_{-d}^n v dz,$	(5)
--------------------------------	--------------------------------	-----

where d is the still water depth

2.4 Roughness Coefficient

The geometry and characteristics of the solid boundaries (e.g. river banks, river bed, and floodplain surface) in NHMs can only be represented to a limited accuracy in a computational grid, and certainly no up to a detail of the bed material. Thus, roughness coefficients are applied to account for the non-resolved momentum and energy losses resulting from the interaction of the flow with the wetted perimeter. This interaction is generally influenced by the channel shape (e.g. degree of sinuosity), cross-section geometry, bed material, vegetation and other flow obstructing elements within the channel (e.g. boulders), as well as by water depth, flow regime and turbulence (Horritt, Bates, and Mattinson 2006; Fisher and Hugh 2003).

Roughness coefficients are used in 1-D, 2-D and 3-D NHMs, but depending on the dimensionality of the model the coefficient incorporates different physical phenomenon. Therefore, the “correct” or most suitable value for the coefficient varies with the model’s dimensionality. Generally, with decreasing dimensionality, the physical phenomenon accounted for by the roughness coefficient increases, leading to potentially higher model sensitivity for variations in the magnitude of the parameter (Wright and Crosato 2011). In a 1-D model the roughness parameter typically incorporates in addition to the flow resistance exerted by the solid boundaries and the vegetation, other physical processes which are not directly represented by the model such as secondary circulation and the effects of horizontal velocity variations. In 2-D/3-D models these physical processes are either directly resolved on a fine enough grid, or are represented by a separate turbulence model (Wright and Crosato 2011).

As flow resistance is a function of the river geometry, the value of a suitable roughness coefficient depends on the way the geometry is represented within the model. As a result both the mesh resolution and the resolution of the topographic data influence the roughness coefficient. Hence, in 2-D or 3-D NHMs the roughness coefficient may be used to

compensate for processes or features not captured by the mesh resolution or the topographic data (Pappenberger et al. 2006).

Roughness coefficients typically vary with the water depth. Increasing water level can lead to both a decrease in the flow resistance due to a lower impact of the bed roughness, but can also result in an increase of the resistance e.g. when the flow reaches more densely vegetated parts of the river (Habersack et al. 2007). Moreover, flow resistance exerted by the vegetation is besides the type, density, distribution and development stage of the vegetation influenced by seasonal variations and the flow velocity. The reason for the latter is that plants tend to become deformed with increasing magnitude of the flow rate (Wright and Crosato 2011). The influence of buildings on the flow can also be accounted for through the roughness coefficient, or alternatively they may be excluded from the computational domain by internal closed boundaries (Habersack et al. 2007).

The determination of the roughness coefficient is usually associated with a high degree of uncertainties as it cannot be directly measured. Hence, the estimated coefficient value is usually optimized during a calibration to minimize errors in the simulation results (Habersack et al. 2007; and Pappenberger et al. 2006).

3. The Numerical Solution

At the first step of a numerical approximation a discretization has to be performed. This is the process of converting the initial partial differential equations to algebraic equations for specific points in the computational space. Most of the numerical methods for the approximation of instationary solutions to the Navier-Stokes equations are based on a separated discretization in space and in time – referred to as the method of lines. Hence, first the spatial discretization is performed leaving the time variable continuous. The time-dependent equations are then advanced in time from a known initial solution by using a suitable method. The method of lines has the advantage of allowing the use of numerical schemes of different accuracy for the spatial and temporal derivatives (Blazek 2001).

There are generally three main method groups used for the spatial discretization of the Navier-Stokes equations: The finite difference method (FDM), the finite element method (FEM) and the finite volume method (FVM). The main criteria for the selection of a certain numerical method are accuracy, robustness and computational costs (Chung 2002).

All of these methods rely on a computational grid which divides the continuous physical domain into a number of non-overlapping contiguous elements.

3.1 Grid Generation

The accuracy of a numerical model is highly dependent on the quality of the computational grid and its ability to represent the domain geometry. This explains why usually more than 50 % of the time of an entire CFD project is spend on the grid generation (Versteeg and Malalasekera, 2007). The accuracy of the numerical solution is dependent on the number of elements in the grid, where a larger number of elements generally results in a higher solution accuracy. However, with increasing number of cells for a given domain, also the computational costs with respect to necessary computer hardware and required calculation time increases. The basic challenge of grid generation is therefore, to find a suitable compromise between desired accuracy and efficiency (Habersack et al. 2007). Elements of a computational grid must cover the entire domain without overlapping. Furthermore, elements should be as regular as possible, i.e. drastic changes in the areas of the elements should be avoided (Blazek, 2001). Generally, it can be distinguished between structured and unstructured grids.

3.1.1 Structured Grids

Structured grids represent a matrix of elements, i.e. they contain planar elements with four edges. Hence, structured grids are characterized by a constant number of elements within one spatial direction, and each element is uniquely specified by an index pair and the corresponding Cartesian coordinates. Thus, for each element the containing nodes and the neighboring elements are given and can be easily accessed. This gives rise to the advantages of relatively fast computation times and low memory capacity requirements. The disadvantage is that structured grids have a low geometric flexibility which is often insufficient for the representation complex features (Rutschmann in Habersack et al., 2006, Blazek, 2001).

3.1.2 Unstructured Grid:

In an unstructured grid, elements as well as nodes have no particular ordering and a unique identification of elements through indices is not possible. Hence, the number of neighboring elements is not defined, and the nodes forming the elements are not fixed from the beginning.

Unstructured grids require therefore in addition to the nodes and their coordinates, information on how these nodes are connected to form the individual elements. They offer a high geometric flexibility and are therefore suitable for the representation of complex geometries. Unstructured grids can be used for the FEM and the FVM (Rutschmann in Habersack et al., 2006, Blazek, 2001).

3.2 The Finite Difference Method

The FDM is one of the oldest numerical approaches to the solution of differential equations, and it was first applied by Euler in 1768. The FDM directly uses the differential form of the governing equations. Taylor expansion series are utilized to approximate the derivatives of the unknown flow variables at discrete grid points. The result is a system of difference quotients at each node of the grid. The FDM allows for a fast computation of high-order approximations, but it can only be applied on structured grids which makes it only suitable for simple geometries (Chung, 2002; Blazek, 2001).

3.3 The Finite Element Method

The FEM uses the integral form of the governing equations. The transformation of the differential form into the equivalent integral form can be achieved either by the variational principle or the method of weighted residuals, which is also known as the weak formulation. For the first, shape functions are used to represent the variation of the solution within an element, outside the given element the value of the shape functions is zero. For the weak formulation, unknown flow variables are approximated within each element and the contribution of all elements is then evaluated over the entire domain through integration. In this way, it is ensured that the weighted average of the residual (i.e. the error of approximation) is zero on the domain level. That is, the relevant conservation laws are obeyed globally. The FEM leads generally to a higher accuracy compared to the FVM, but is computationally more expensive (Rutschmann in Habersack et al., 2006, Blazek, 2001).

3.4 The Finite Volume Method

The FVM is the numerical method which is used by the software package employed for the case study of this thesis. Thus, it will be explained in greater detail than the previously described methods.

The FVM is based on the integration of the governing PDEs over defined control volumes within the computational domain. The integral formulation is then approximated by evaluating the fluxes across the boundaries of these control volumes. As a result, the fluxes are discretized and a set of algebraic balance equations for discrete flow variables is defined for each control volume. Hence, the FVM satisfies the conservation laws locally, i.e. at each element (Versteeg and Malalasekera, 2007). The method can be employed on both unstructured and structured grids making its application suitable for both complex and simple geometries. Compared to the FEM, the FVM is of lower accuracy, but requires less computational effort. There are two main schemes for defining the control volumes and the location of the flow variables: the cell-vertex scheme and the cell-centered scheme. The first one, stores flow variables at the grid points, and the control volume is established around this grid point. The cell-centered scheme on the other hand, stores flow variables at the centroids of the grids cells, and the control volume is identical to the grid cell (Blazek, 2001).

4. Topographic Data for NHMs

For the construction of a 2-D river flood model, data describing the river channel bathymetry and the topography of the surrounding floodplains has to be available. The quality of topographic data for a river model in terms of spatial resolution and vertical accuracy are generally determined by the technique used to obtain the data and by the applied processing measures (e.g. interpolation or filtering algorithms). Independent of the type of interpolation routine employed, the quality of the produced surface is mainly influenced by the following factors (Merwade et. al 2008):

- Distance between the measured points
- Density of the measured points
- Orientation of measurements (parallel to the flow direction or perpendicular to it)
- Distance between cross-sections
- Availability of further topographic information (i.e. breaklines)

4.1 Methods for Data Collection

Commonly applied methods for the data collection of NHMs include photogrammetry and airborne Light Detection and Ranging (ALIDAR) for the floodplains, and field surveying,

echo sounding as well as laser bathymetry for the river channel (Mandlbürger 2009). These methods will now be briefly described and compared.

4.1.1 Photogrammetry

The photogrammetric evaluation of aerial photographs offers a suitable method for the production of DEMs for large areas which are preferably only sparsely vegetated. The vertical accuracy ranges between 15 and 100 cm, and the average distance between points is usually between 10 and 50 m. However, due to the advancements in ALIDAR, photogrammetry is nowadays only rarely applied for the data collection of NHMs (Habersack et al. 2007; Mandlbürger 2009).

4.1.2 Light Detection and Ranging

ALIDAR has become to the most important method for data acquisition in the field of high resolution DEMs. ALIDAR systems measure elevations through determining the travel time of at the surface reflected light pulses which are emitted by sensors attached to an aircraft or satellite. This allows with the aid of a GPS system and an inertial measurement unit, the collection of a dense array of geographic coordinates (Habersack et al. 2007; Reutebuch et al. 2003). The density of the measured points is determined by the frequency of the emitted signals, and generally ranges between one and ten points per m². The vertical accuracy of the measured points is usually between 10 to 20 cm (Wright and Crosato 2011). Highest accuracies can be achieved on flat and open areas where light signals are reflected at the surface ground only. On densely vegetated areas (i.e. forests) on the other hand, the accuracy might be reduced due to the difficulty of distinguishing between ground- and off-ground reflections. Hence, LIDAR measurements should be preferably conducted during vegetation free seasons (Reutebuch et al. 2003). However, the high resolution of remotely sensed data often results in data volumes too large for direct use within numerical models. Therefore, in many cases methods of data reduction have to be used to trim down the data volume to an acceptable level while preserving the important features of the area (Mandlbürger 2009).

In addition to the importance of accuracy of the data, for a river model it is essential that the available data captures hydraulic significant features such as the water-land-boundary and dikes. However, raster based LIDAR data may not sufficiently represent these features, and hence it may be necessary to use additional data e.g. from field surveying methods

(Habersack et al. 2007). In addition to offering accurate data for the topographic description of the model domain, remotely sensed data can also give information about inundation extends, which can be used for the validation and calibration flood models (Wright and Crosato 2011).

4.1.3 Field Surveying Methods

Field surveying techniques are the traditional way of collecting river bathymetry data. Tachymeters, GPS-systems and other tools provide measurements of high accuracy (ca. 1cm), but their application for extensive large-scale topographic descriptions is economically not feasible. A further constraint is that their application is limited to shallow rivers. Hence, they are mainly used for measuring elevations along cross-sections of smaller rivers. The distance between these cross-sections is selected with respect to geometric variability of the river, and commonly ranges between 50 and 150 m. Field surveying methods are suitable for collecting the data input of 1-D models, but can also be used for creating supplementary high accuracy data for 2-D models (Habersack et al. 2007; Mandlbürger 2009).

4.1.4 Echo Sounding

Echo sounding is a hydroacoustic technique used to collect bathymetry data through sound impulses. The technique measures the period of time between the emissions of a sound pulse and the reception of its echo. The water depth is then calculated with the known speed of propagation of sound through water. The echosounder is attached to a vessel that is additionally equipped with a GPS receiver for associating the measured depth with a geographic location. The density of measured points is dependent on the type of echosounder used, which can be classified into single beam, multi-single beam and multi beam echosounder. The first two measure water depth perpendicular to the transmitting device, and thus, produce a series of parallel cross sectional bathymetry recordings which are usually aligned along the direction of the flow. A multi beam echosounder on the other hand emits acoustic signals simultaneously in several directions, and therefore allows a planar data capturing of the river bed (Habersack et al. 2007). The swath coverage of the multi beam echosounder increases with distance, and they are therefore optimally used in deep waters, whereas their effectiveness in shallow waters can be low. Furthermore, echo sounding systems in general cannot measure up to the land-water boundary which may require the use

of supplementary data capturing methods for the description of the river banks (Banic and Cunningham 1999).

4.1.5 Laser Bathymetry

Another method for large scale bathymetry data collection is Airborne Laser Bathymetry (ALB), which is based on the same principle as the previously described ALIDAR, but emits laser impulses of two different wavelengths: one ($\lambda \sim 1064$ nm) which is reflected at the water surface and another one ($\lambda \sim 532$ nm) which penetrates the water column, and is reflected at the bed level. The water depth can therefore be determined from the difference in the time of flight of the two (Habersack et al. 2007). ALB is applicable in very shallow waters (<5 m), and is capable to survey both water and land at the same time providing a continuous description at the land-water interface. The vertical accuracy of an ALB is typically higher than 20 cm, and its horizontal position accuracy is better than 1.5 m. However, the maximum measured water depth with ALB is limited by the water clarity, and ranges for the usually rather turbid inland waters only between a few meters to a maximum of 20 m (Banic and Cunningham 1999).

4.2 Data Formats for the Representation of Surfaces

In GIS there are generally three possibilities to represent surfaces which include contour or isolines, triangulated irregular networks (TINs) and cell-based raster surfaces (Weih Jr 2010). A model which describes the surface elevation for a given area is commonly termed digital elevation model (DEM):

The term DEM is not clearly defined, and it is often used interchangeably with the terms digital terrain model (DTM), or digital surface model (DSM). But, one can define a DEM generally as a mathematical description of the Earth's surface in a digital form. It usually represents the topography of the bare earth without vegetation or human made structures. Nevertheless, while buildings are usually not represented in a DEM, other structures which do not significantly elevate above the ground level (e.g. roads) are included. In river-floodplain models, flow obstructing elements which are not incorporated in the available topographic data are often indirectly accounted for through roughness coefficients (Mandlbürger 2009).

Most commonly, the mathematical description of a DEM is in the form of a bivariate function (i.e. $z = f(x, y)$) which assigns an elevation to any point in a given 2-D space, where the z-value is usually given perpendicular to the surface. This type of DEM, which is referred to as 2.5-D-DEM, provides a sufficient approximation of the surface elevation for most applications, although, it does not preserve the exact vertical shape of features. A fully 3-D-DEM might be e.g. necessary for numerical hydrodynamic models where bridges have to be represented correctly (Mandlbürger 2009). In order to adequately describe discontinuities, a DEM can be supplemented by breaklines which basically divide a domain into independent interpolation areas. In this way important linear features such as dikes or mountain ridges can be properly described. Common errors of DEMs are sinks which are depressions within the modeled surface. Although sinks can occur naturally, many of them are due to an erroneous representation of the DEM which results e.g. from the rounding of elevations (ESRI 2012). A DEM can be in the form of a raster or a TIN where the data for both is usually obtained with remote sensing- or land surveying techniques.

4.2.1 Raster based DEMs

Rasters are the most common data structure of DEMs since elevation data is frequently available in this format. They consist of a matrix of cells arranged in columns and rows where each cell contains a z-value. The spatial resolution of a raster is generally determined by the dimension of its cells, where with decreasing cells size the level of detail and the smoothness of the raster increases. Clearly, with increasing number of cells also the demand in storage capacity and the time required for processing increases. It has to be considered that features of a surface smaller than the cell size may not be captured by the raster. Hence the cell size of a raster should be small enough to represent the required level of detail, but large enough to allow for an efficient storage and analysis of the data. Naturally, it is possible to simplify any raster into a raster of a lower resolution, while the opposite is not achievable. Furthermore, rasters often do not preserve linear features of an area (ESRI 2012; Mandlbürger 2009).

4.2.2 Triangular Irregular Networks

A TIN consists of vector data which divide a surface into a network of non-overlapping, contiguous triangular elements of varying size and shape. The triangles are formed by linking a set of 3-D points which can be obtained through direct measurement or through the

extraction from a DEM. Through interpolation of the thereby formed vertices or nodes, the z-value for any point within a TIN is given. Thus, the precision of the input points is preserved while the values between them are modeled. The most commonly used method for the triangulation is the Delaunay triangulation which is based on the criterion that the circumcircle of any triangle does not contain an additional node besides the three nodes forming the triangle. As a result of this, the minimum interior angle is maximized for every triangle, and the construction of long, thin triangles is prevented to a maximum degree (ESRI 2012). Thereby, the distance of any point on the surface to a node is minimized. ArcGIS which is used for the case study of this thesis employs the Delaunay criterion.

Since TINs can be created from irregularly distributed points, the density of nodes can be selected to vary according to the variation in the described surface. This allows having high resolutions (i.e. high density of nodes and small triangles) in areas where the variation in height is intense or where a detailed representation of the surface is required, whereas flat or unimportant areas can be represented by only a few nodes and large triangles (ESRI 2012).

An advantage of TINs is their ability to accurately describe linear features which are topographically important for a given surface as a sequence of triangle edges. The preservation of a linear feature, such as a river bank, a ridge, or a dike within a TIN can be ensured by using so called breaklines, which can be classified as either hard or soft. Hard breaklines induce a discontinuity in the slope of a surface and are used to account for abrupt elevation changes. Soft breaklines on the other hand force triangle edges along a linear feature but do not affect the local slope (ESRI 2012). Moreover, due to its ability to contain multiple levels of resolution, a TIN offers a high efficiency in storing as the number of vertices can be reduced in areas of low terrain variability (Vivoni et al. 2004). However, compared to raster surface models, the construction and processing of TINs is more expensive due to a higher complexity of their data structure (ESRI 2012).

5. The Applied Modeling Tools

5.1 Mike 21 Flow Model FM

For the case study of this thesis the software package Mike 21 Flow Model FM (M21fm) was used. M21fm was developed by Danish Hydraulic Institute (DHI) for the 2-dimensional simulation of flows, sediment transport, waves and ecology in coastal areas, estuaries, lakes

and rivers. The simulation of hydrodynamic processes is performed through the numerical solution of the depth-integrated incompressible Reynolds averaged Navier-Stokes equations (i.e. the two-dimensional SWEs). In the horizontal domain both Cartesian and spherical coordinates can be used (DHI 2007). The spatial discretization of the partial differential equations within M21fm is based on a cell-centered FVM applied on an unstructured grid. For this the computational domain is divided into a grid of non-overlapping elements in the form of triangles or quadrilateral elements. The convective fluxes at the faces of the control volumes are computed by using an approximate Riemann solver (DHI 2007).

For the time integration Mike21fm applies an explicit scheme. Thus, due to the stability restriction using an explicit scheme, the time step interval must be selected so that the Courant-Friedrichs-Lewy (CFL) number is less than 1. The CFL number is formulated for the SWEs as:

$$CFL_{HD} = (\sqrt{gh} + |u|) \frac{\Delta t}{\Delta x} + (\sqrt{gh} + |v|) \frac{\Delta t}{\Delta y} \quad (6)$$

Δx and Δy are the characteristic length scale of an element of the computational grid. They are determined by the minimum edge length of an element. The water depth h and the velocity components u and v are calculated at the center of each element.

In order to allow any numerical method to solve the given governing equation within the discretized computational space suitable boundary and initial conditions have to be specified.

5.1.1 Boundary Conditions

Boundary conditions influence the accuracy of the simulation results, and they affect both the stability and the convergence speed of the numerical solution (Blazek, 2001). One can distinguish between three types of boundary conditions: closed boundaries, open boundaries and moving boundaries.

Closed boundaries represent the natural fluid-solid boundaries of the physical domain. At these land boundaries the normal component of velocity is forced to zero.

$$\vec{v} \cdot \vec{n} = 0$$

Furthermore one can distinguish between full slip and no slip conditions at land boundaries. The difference between the two is that the later assumes the tangential velocity component to be zero due the influence of viscosity. The Mike Zero mesh generator by default specifies full slip conditions for closed boundaries, but no slip conditions can be applied as well (DHI, 2007).

Open boundaries are the artificial fluid-fluid boundaries set by the modeler through cutting down the domain to a size appropriate for the given study. For a numerical model of a river, the boundaries should optimally be located at places where measured data is available. For the specification of hydrodynamic boundaries there are three options in M21fm (DHI, 2007):

- Specified water level
- Specified discharge
- Specified fluxes

Additionally, M21fm offers a “soft start” option, which is a user defined period of time in which boundary conditions are gradually increased starting from zero (DHI, 2011).

The moving boundaries (e.g. the free water surface) are defined by the hydrodynamic processes within the domain. The treatment of moving boundaries within M21fm is based on an approach of Zhao et al. (1994) and Sleigh et al. (1998). This approach evaluates the water depth in each grid element and classifies them according to a certain tolerance depth as wet, dry, or partially dry. When the water depth is less than the specified tolerance depth (h_{dry}), the element is classified as dry and is removed from the calculation. This implies also the removal of water from the computational space, but the water depth is stored and re-inserted once the element becomes flooded again. Conversely, an element is classified as wet when the water depth is larger than h_{wet} . For wet elements both mass fluxes and momentum fluxes are computed. An element is considered as partially dry when the depth is greater than h_{dry} and less than h_{wet} , or when one of the element faces is a flooded boundary. For partially dry elements the momentum fluxes are set to zero, and only the mass fluxes are calculated. In order for an element face to be defined as flooded, water depths at one of the element faces must be less than h_{dry} , while at the other face water depth must be larger than a defined value (h_{flood}). Furthermore, the sum of the still water depth at the h_{dry} face and the surface elevation at the other face must be greater than zero. Elements which are considered as being

flooded are re-entered into the calculation. For the magnitudes of the different tolerance depth the following relation must be satisfied (DHI, 2007):

$$h_{dry} < h_{flood.} < h_{wet}$$

5.1.2 Initial Conditions

For the numerical solution of hydrodynamic problems initial conditions have to be defined. Initial conditions specify the state of the fluid at all computational nodes prior to the start of the simulation period, and they influence the stability of the numerical scheme as well as the time the model requires to converge towards realistic predictions (Blazek 2001). In order to avoid numerical breakdowns at the beginning of the simulation the initial conditions of the model should be in rough accordance with the specified boundary conditions. In case of a river model that means e.g. to ensure a smooth transition between the inflow and the specified downstream water levels. Correct initial conditions are particularly important in cases where accurate solutions are required directly from the beginning of the simulation. This can be achieved with a so called “hot start”, which is basically to use the results of a previous simulation as initial conditions (DHI 2011).

5.2 Mike Zero Mesh Generator

The computational grid of the domain was created with the MIKE Zero Mesh Generator (MZMG) which is a tool for creating and modifying unstructured grids consisting of triangular or quadrangular elements or a combination of both (DHI 2011).

The generation of a grid within the MZMG proceeds generally in the following way: First, the model domain has to be defined through polygons which enclose the area of interest. Within these polygons a triangulation is then performed to divide the continuous computational domain into discrete elements for which the discrete formulations of the governing equations can be solved for the unknown flow variables. This depth independent grid is then associated with z-values by an interpolation of the topographic points (referred to as scatter data in the MZMG) onto the nodes of the grid.

For the generation of the triangles the MZMG employs the code “Triangle” which was developed by Jonathan Shewchuk (DHI 2009). Triangle allows to place constraints on the

maximum triangle area of a grid, and it uses an algorithm which avoids small angles while keeping the element number relatively low (Shewchuk 1996).

There are three user-defined parameters within the mesh generator to specify the triangulation (DHI 2011):

1. The maximum allowable element area
2. The smallest allowable angle between two edges of the triangle
3. The maximum number of used nodes

After triangulation the smoothing function of the MZMG can be applied. This function ensures an improved applicability of a mesh in a simulation by re-positioning the created nodes in order to maximize element areas and angles. This process can however result in a grid which deviates from the initially defined triangulation parameters (i.e. minimum angle and maximum element area). A description of the smoothing procedure is found in the scientific manual of the mesh generator (DHI 2009).

The MZMG offers two options for the interpolation of the topographic data onto the triangular elements namely the natural neighbour and linear interpolation. For the interpolation of quadrangular grids furthermore a modified version of the inverse distance method can be applied.

The MIKE Zero Mesh Generator distinguishes between closed and the different open boundaries through the definition of attribute values for each node in the grid. The attribute value “1” is used for all land-water boundaries, and open boundaries are identified by a value greater than “1”. As the Mesh Generator defines by default all boundaries as land boundaries, only the open boundaries have to be defined.

6. The Case Study

6.1 The Study Area

The river Rhine is one of the economically most important rivers in the world (Thu, Goebel, and Nestmann 2002). It has a total length of ca. 1,230 km and its average discharge as measured in Cologne is 2,090 m³/s (Koppe 2012; BFG, 2012). From its source in the Saint-Gotthard Massif of the Swiss Alps, it flows through Austria, Germany and the Netherlands

where splits into the Waal and the Pannerden Canal. The catchment of the Rhine covers an area of about 185,000 km and is part of nine European countries (Koppe 2012). The main river channel is commonly classified into six parts: The Alpine Rhine, the High Rhine, the Upper Rhine, the Middle Rhine, the Lower Rhine and the Delta Rhine. Predictions estimate an increasing discharge in the river Rhine due to climate change, which would increase the risk of flooding along its course (Hesselink et al. 2003).

The hydrodynamic model will be created for an approximately 33 km long section of the Lower Rhine stretching from the towns Ruhrort in the South to Wesel in the North. The dike breach and the resulting flood inundation will be simulated for the polder Mehrum. The polder is a former floodplain of the Rhine which is prevented from being inundated through dikes. Within the polder there are three main residential areas namely Mehrum, Löhnen and Götterswickerhamm.



Figure 1: The river Rhine (germanwineroute.com)

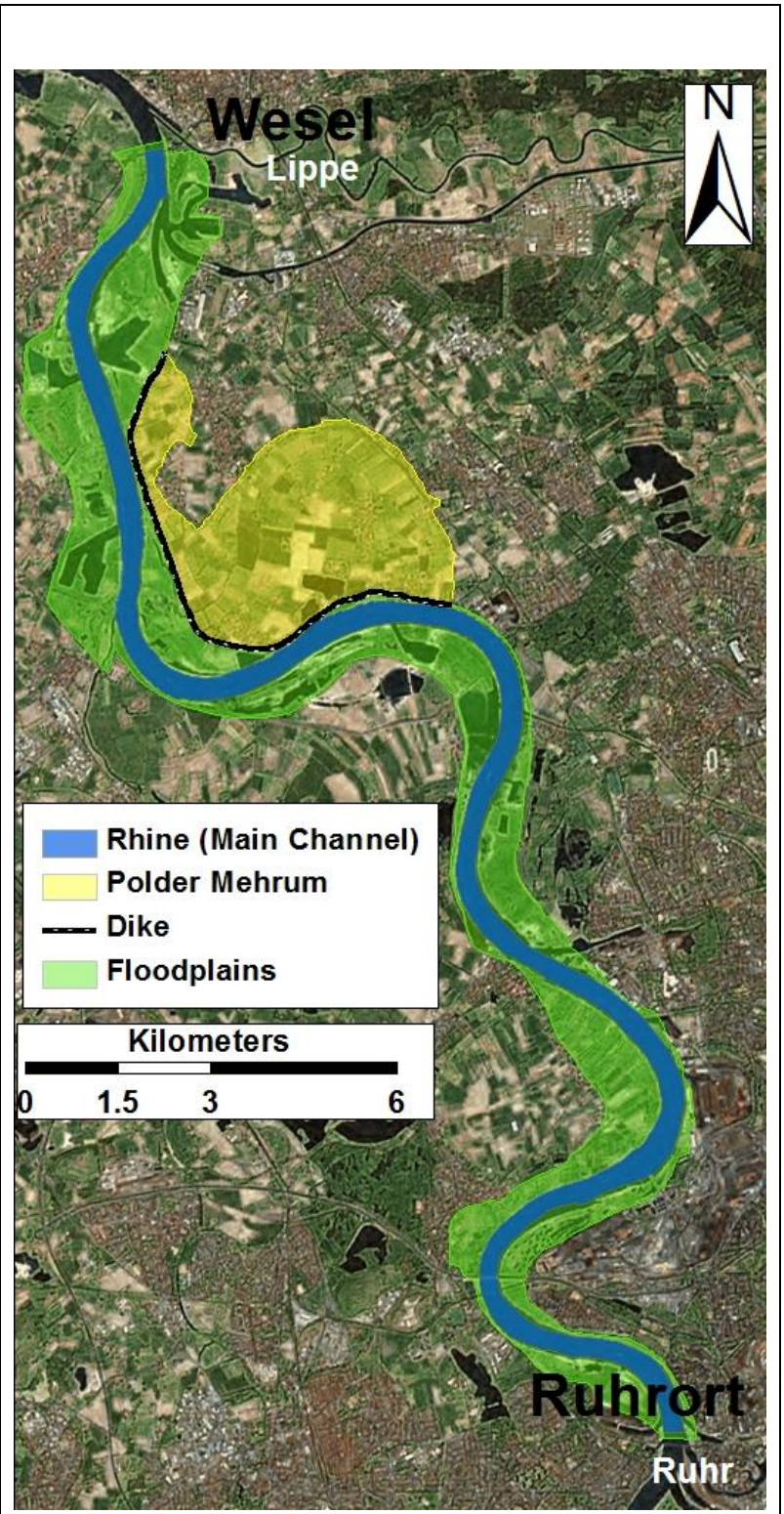


Figure 2: The study area (Source: Bing Maps Aerial)

6.2 The Simulated Flood Event

A flood which took place from the 7th of January to the 25th of February in 1995 will be simulated. The flood event was initiated by snowfall and winter conditions during the first week of January which led to an accumulation of snow cover, particularly in the Mittelgebirge. A subsequent rise in temperature and the connected partial melting of the snow cover as well as rainfall on the Rhine catchment resulted in highly reduced water storage capacities of the soil. The flood was finally caused by an intensive rainfall period which occurred from the 22nd until the 30th of January combined with a melting of almost the entire snow cover in the Mittelgebirge.

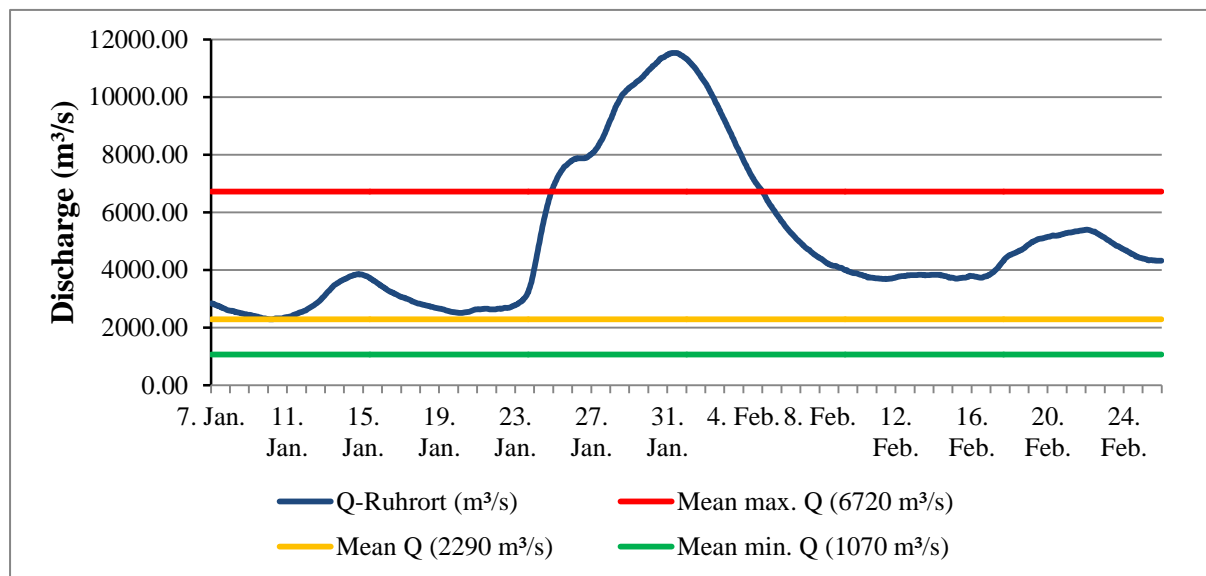


Figure 1: 1995 flood event, discharge at Ruhort (Source: BFG, 2012)

This resulted in extreme discharges in the river Rhine which peaked on the 31st of January to 11,600 m³/s at Ruhort. This magnitude is only slightly lower than the highest ever recorded discharge of the Rhine which occurred in January 1926 (Chbab, 1996; BFG, 2012). Statistically, the peak discharge of the 1995 flood is located between a 50- and 100-year flood event which have peak flows of 11,380 m³/s and 12,400 m³/s respectively (BFG, 2012).

6.3 Available Topographic Data

The available topographic data for the river model consists of a text file containing the coordinates (xyz) of ca. 150,000 measured points together with the corresponding river kilometer. The points were measured as straight lines perpendicular to the main channel at an interval of approximately 100 m, and are given in the Gauss-Krüger coordinate system. They

extend from Ruhrort (Duisburg) in the North, where the Ruhr enters, to Wesel in the South, where the Lippe enters the Rhine. This results in coverage of ca. 34.4 km of the river Rhine. Two stream gauges fall within this river section—one in Wesel and the other one in Ruhrort (BFG, 2012). The width of the cross-sections ranges from ca. 400 to 2,500 m and the elevation ranges from ca. 5 to 47 m. The source of the data as well as the method used for obtaining them is unknown which makes it difficult to judge the quality of the data

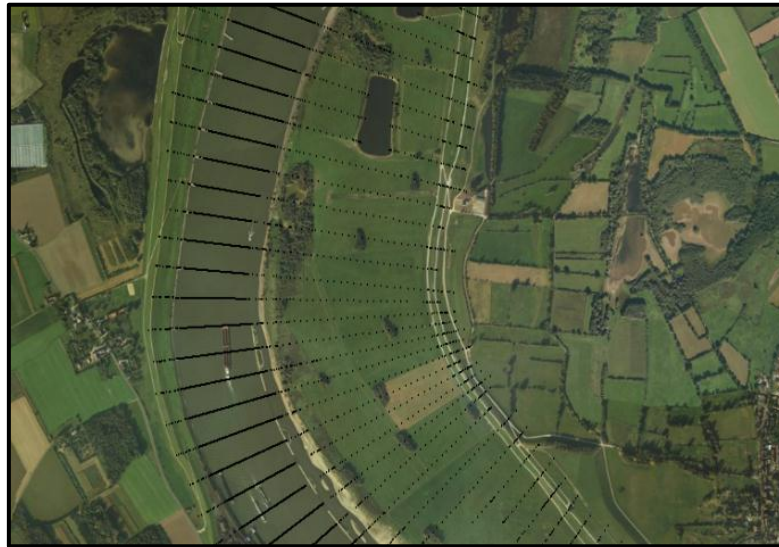


Figure 2: Available topographic data on a satellite image (Source: Bing Maps Aerial, 2012)

The graphical representation of the points within ArcGIS revealed a few gaps within the otherwise rather regularly distributed data. However, as an overlay with a map of the main channel shows, these gaps are not located within the main channel and do therefore not pose a significant problem. Through individual measurements, the horizontal distribution of the measured points is estimated to vary between approximately 30 and 1 m. The closest distribution of points is found along the main channel and at the river curves (Figure 2). The distance between points of the same cross-section within the main channel is between 1.4 and 0.1 m.

The cross-sectional oriented measurement of data, i.e. a relatively dense distribution of measured data within a cross-section compared to a large distance between two cross-sections, is common for rivers. This measurement approach for rivers is in most cases acceptable since the topographic variation in the direction of the flow is due to the erosive force of the water rather small (Mandlbürger 2009).

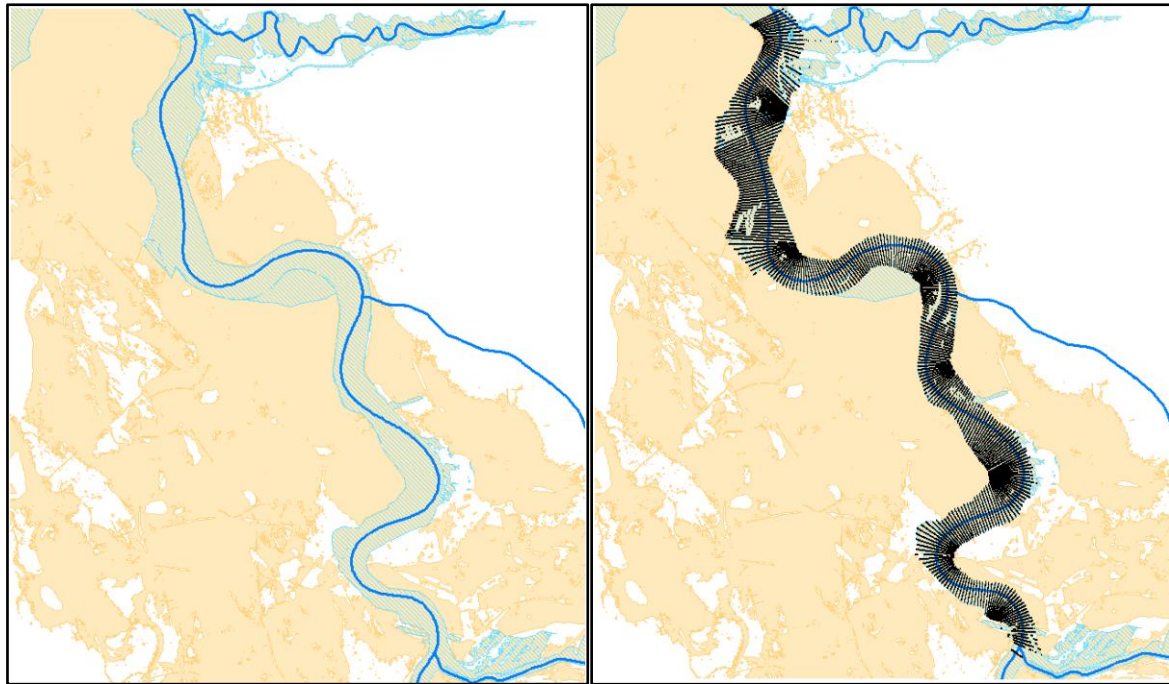


Figure 3: Inundation areas for HQ500 with dikes (blue) and without dikes (beige; Source Geoserver NRW, 2012).

In order for the model to predict a realistic inflow into the polder, all relevant floodplains along the river section should be included in the model. To investigate whether the floodplains are covered by the available data, a map showing the estimated inundation areas for a 500-year flood was used (Figure 3). The map shows the flood extend for both a scenario with the existing dikes (light blue) and a scenario without dikes (beige). This reveals that the measured points essentially stretch over the complete area of the floodplains. Thus, with regard to the vertical spatial extension, the available topographic data proved to be suitable for the purpose of investigating a flooding event.

7. Creation of the Numerical Hydrodynamic Model

An unstructured computational grid of the river and the connected floodplains was created from the available topographic data. This involved the definition of the model boundaries, a triangulation of the nodes within these boundaries and an interpolation of the topographic data onto the created grid elements. Several grids with different amounts and distribution of nodes were created to identify the most suitable one in terms of accuracy and computational time. Measured flow data of the selected flood event were then introduced to the open boundaries, initial conditions were defined and various simulation parameters were specified. A simulation of the hydrodynamic processes within the river under non-breaching conditions was run to compare the obtained simulation results with the corresponding measured data.

Modifications of the grid as well as of the roughness coefficient were performed until an acceptable match between the two was achieved. Subsequently, the polder area was included into the computational domain. This was done by extracting a suitable amount and distribution of 3-D points from a DEM of the area. Moreover, it was ensured that the dike separating the polder from the river was fully accounted for in the model so as to avoid flooding of the polder during non-breaching conditions.

7.1 The Grid Generation

A computational grid should be designed according to the desired accuracy of the results and the affordable computational expenses. The influence of the grid on the accuracy of the numerical results is mainly determined by two general aspects: One is the quality of the available topographic data with respect to resolution and spatial distribution. The second one is the way the modeler uses this data to create a continuous representation of the topography. This particularly includes the selection of an interpolation routine which preserves characteristic features of the topography. For a realistic simulation of hydrodynamic processes within a river, the grid has to reflect the topographic features which govern these processes. Thus, it is essential to include hydraulically relevant features which naturally influence the flow dynamics. Within an unstructured grid this can be done by distributing the nodes according to geometric variability and significance of the available data, as well as through the introduction of breaklines. Furthermore a data pre-processing step may be necessary to reduce the data volume to an acceptable volume, while preserving the most important information. Finally, the number and distribution of nodes within the domain determines the spatial scale for which the governing equations are solved. Generally, the size of an element within a model determines the smallest spatial hydraulic variations which can be reproduced at this element during a simulation (Horritt, Bates, and Mattinson 2006). The coarseness of the grid in turn has a main influence on the computational costs in terms of hardware requirements and necessary computational time. Hence, a reasonable compromise between simulation accuracy and computational requirements has to be found (Habersack et al. 2007).

7.2 Definition of the Computational Domain

The initial step for the mesh generation was to define the boundaries of the computational domain. This was done within ArcMap 10 by employing the editor function to create a point

feature class around the relevant river section and its adjacent floodplains. For the identification of relevant floodplains, dike lines and surface water bodies along the river section, Bing Maps Aerial as well as different maps provided by the Geoserver NRW were used. In order to use Bing Maps Aerial, which is provided in WGS89, as a background layer a coordinate transformation into the Gauss-Krüger projection had to be used.

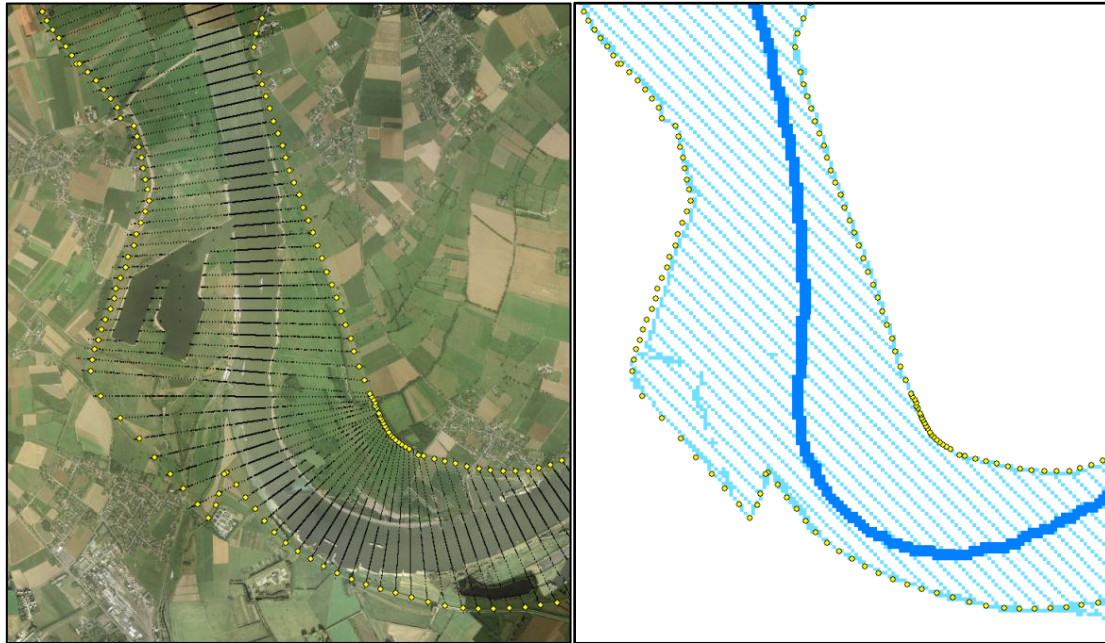


Figure 4: Domain boundary points located at the outer extend of inundation areas for non-breaching conditions (Source Bing Maps Aerial and Geoserver NRW, 2012)

For the simulation of a correct discharge within the main channel and thus, also for a correct prediction of the inflow into the polder under breaching conditions, it is important that the model properly incorporates the areas which are naturally inundated during periods of high discharge. In order to ensure that the full flood retention capacity of the land adjacent to the river section is accounted for in the model, a map which shows inundation areas resulting from a statistically 100-year flood event under the assumption of no dike failures was used. Hence, this assumption, with exemption of a dike breach at the polder Mehrum, holds also true for the applied model. In this way the boundary was essentially created by tracing the dikes along the river. Furthermore, the boundary points, which will serve as nodes for triangulation, are placed in close distance to the measured points so as to achieve a higher vertical accuracy during the interpolation of the z-values.

The open boundaries of the model were created at the locations of the stream gauges from which flow data is available, so as to ensure that these data can be applied realistically.

7.2.1 Upstream boundary

The coordinates and the river kilometer of the stream gauge are known and its location is identified at the beginning of the Hafenmund (Figure 5), which is less than a kilometer downstream from the point where the Ruhr enters the Rhine (WSV 2012). The upstream boundary is created perpendicular to the main channel along the corresponding cross-section at the end of the harbor. The two harbors at the beginning of the river model are only partially included in the computational domain (Figure 6). However, due to their relatively small size, their influence on the later simulated flooding of the Mehrum polder can be assumed as negligible.

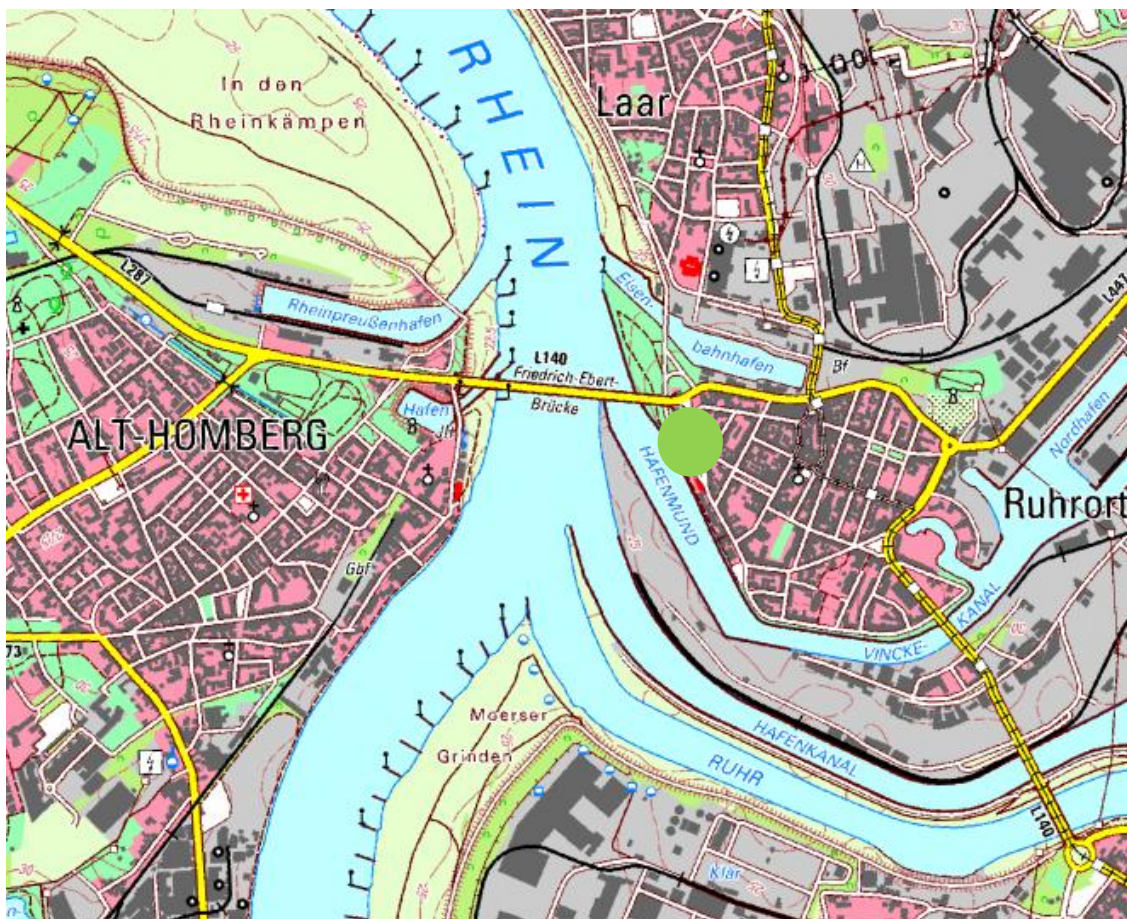


Figure 5: Location of the upstream gauge (green dot) in Ruhrort (Source: Geoerver NRW, 2012)

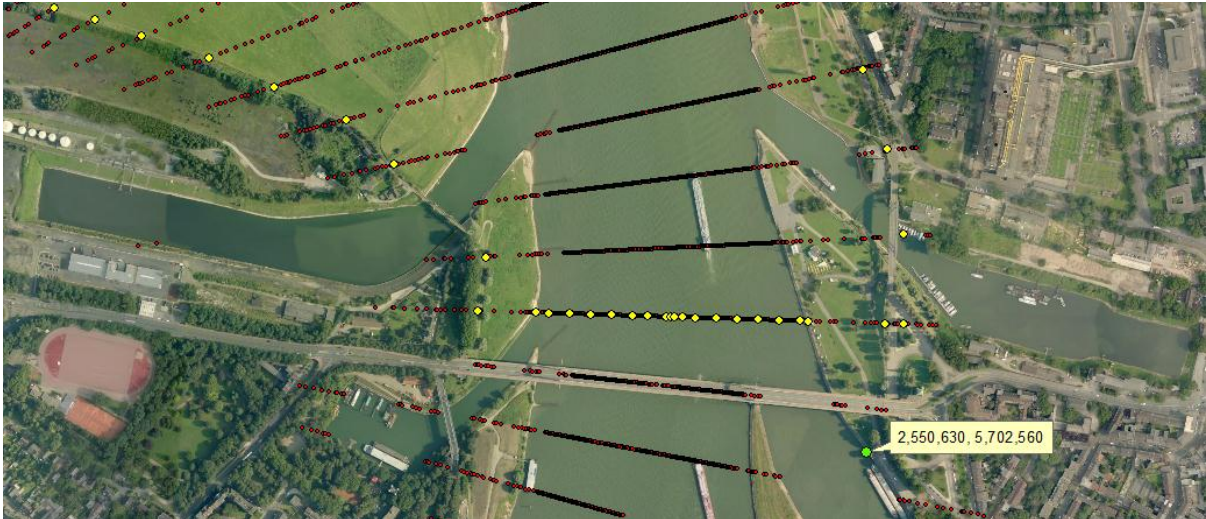


Figure 6: The upstream boundary (yellow dots) created along the measured data close to the stream gauge (green dot) in Ruhrort (; Source: Bing Maps Areal, 2012)

7.2.2 Downstream boundary

The stream gauge is located at the Rhine river kilometre 814.000 which is roughly 300 m upstream from where the river Lippe flows into Rhine (WSV 2012). The boundary is created along the corresponding line of measured data points.

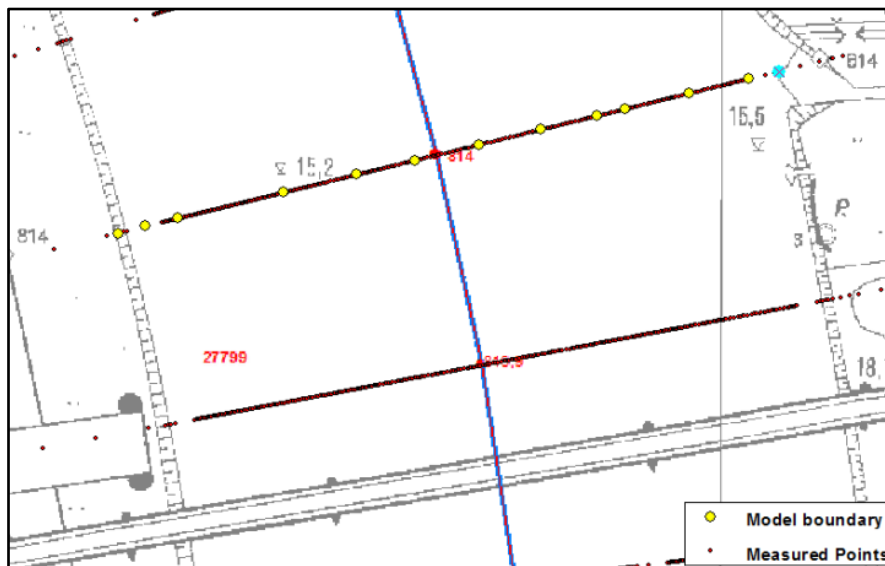


Figure 7: Upstream boundary created at river km 814 along the measured data (Source: Geoserver NRW, 2012)

Less than 1 km upstream of the downstream boundary the Wesel-Datteln-Canal enters the Rhine. Only the part of the canal until the first lock is included in the model domain. Hence, it is assumed that the lock will be closed during a flood event. Before the canal flows into the Rhine it is connected to two harbors which are part of the computational domain. A separate

shape file is created to insert additional nodes at measured points within the harbors and the canal to ensure that these points are accounted for in the model (see appendix).

The complete boundary (Figure 8) encloses an area of ca. 38 km² and covers 33.2 river kilometers. The created shape file of the domain boundaries was converted into an ASCII text file and imported into the MZMG. Node connectivity information was added to allow the mesh generator to create a closed polygon from the file. The boundaries were specified as closed or open boundaries by changing the attribute value of the corresponding polygon sections.

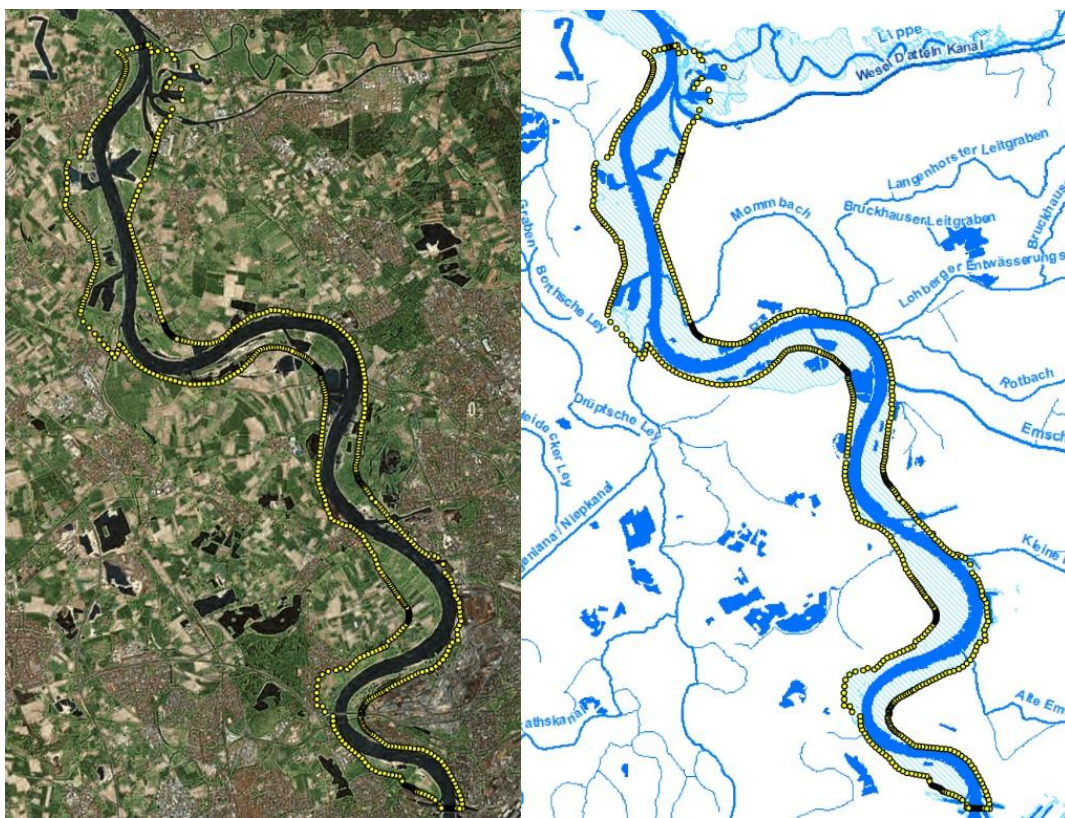


Figure 8: Complete boundary of the computational domain on a satellite image and a flood inundation map (Source: Bing Maps Areal, 2012; Geoserver NRW, 2012)

7.2.3 Representation of the Dike

In order to avoid flooding of the polder Mehrum during non-breaching conditions, the dike separating the polder from the river has to be accurately accounted for in the model. This was done by extracting points located on the dike from a DEM, and by inserting these points as connected nodes into the MZMG. Thereby, the elevation of these points was preserved during interpolation. However, a 3-D visualization with the Mike Animator revealed that the used approach did not result in a continuous representation of the dike. Figure 9 shows the

presence of considerable gaps along the dike. This occurs because the mesh generator introduces additional nodes in order to fulfill the defined mesh criteria (e.g. minimum angle). Since all points surrounding the dike are of a lower elevation, nodes along the dike will usually receive significant too low z-values through interpolation. This problem was solved by manually raising the elevation of each of the introduced nodes to a more realistic z-value after interpolation. The disadvantage of this approach is that the corrected z-values will be lost once interpolation has to be performed again, e.g. in case the mesh is modified. Another possibility would have been to insert two breaklines—one each side of the dike—so that only the thereby enclosed topographic data is considered during the interpolation. However, here it has to be regarded that breaklines significantly increase the time required by the interpolation process.

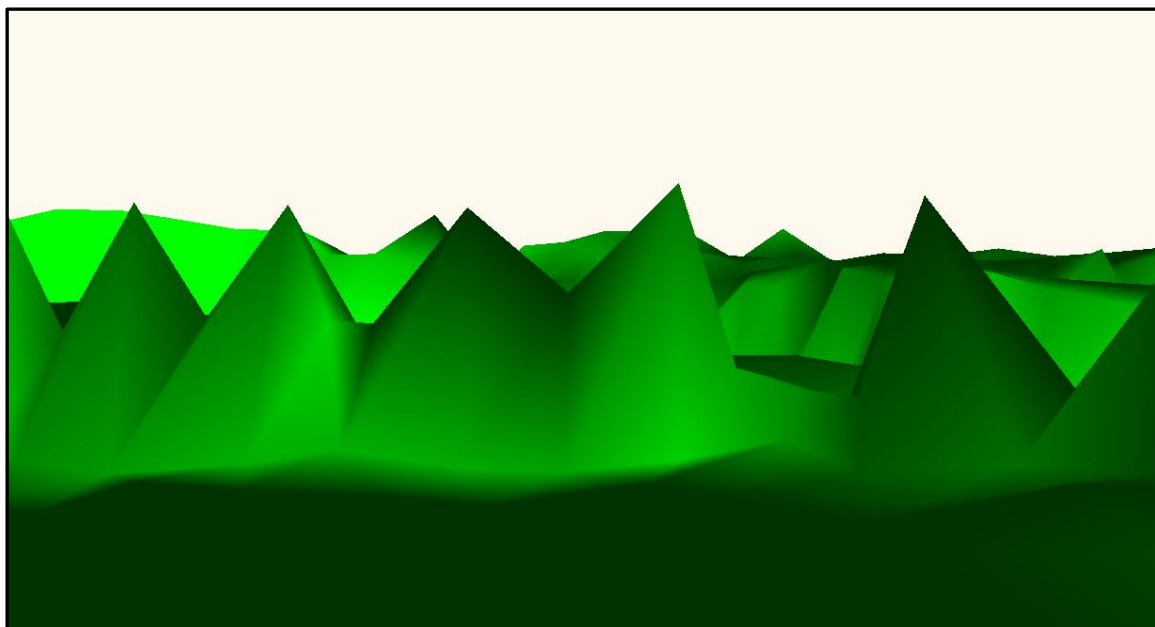


Figure 9: Representation of the dike separating the polder Mehrum from the river before a manual correction of the z-values was performed

7.3 Mesh Resolution

In order to identify a suitable compromise between the mesh resolution and the required simulation time a study was conducted to determine the effect of the mesh resolution on the geometrical representation of the given bathymetry data. This was done by creating a set of meshes of an increasing number of nodes, and by calculating the volume of the resulting surface from a reference plane in ArcMap.

The meshes were created within the MZMG by using a minimum allowable angle of 26 degree and by using a linear interpolation of the measured data onto the nodes. As the minimum number of nodes for the given domain and the specified minimum angle is approximately 1,000, a lower node number could not be used. Additionally the maximum node number which could be processed within the mesh generator was 128,000. As benchmark, a TIN which incorporates all measured points as nodes was created. However, triangulation of the complete set of measured points without any additional nodes resulted in very long and thin triangles in ArcMap. Thus, it is questionable whether the benchmark TIN really represents the maximum topographic accuracy achievable with the given data.

An ASCII file containing the coordinates of the nodes of each mesh was then imported into ArcMap, where it was subsequently converted into a three dimensional point feature class. From these feature classes, TINs were created which are clipped to the relevant domain by using a polygon of the model boundary (Figure 10).

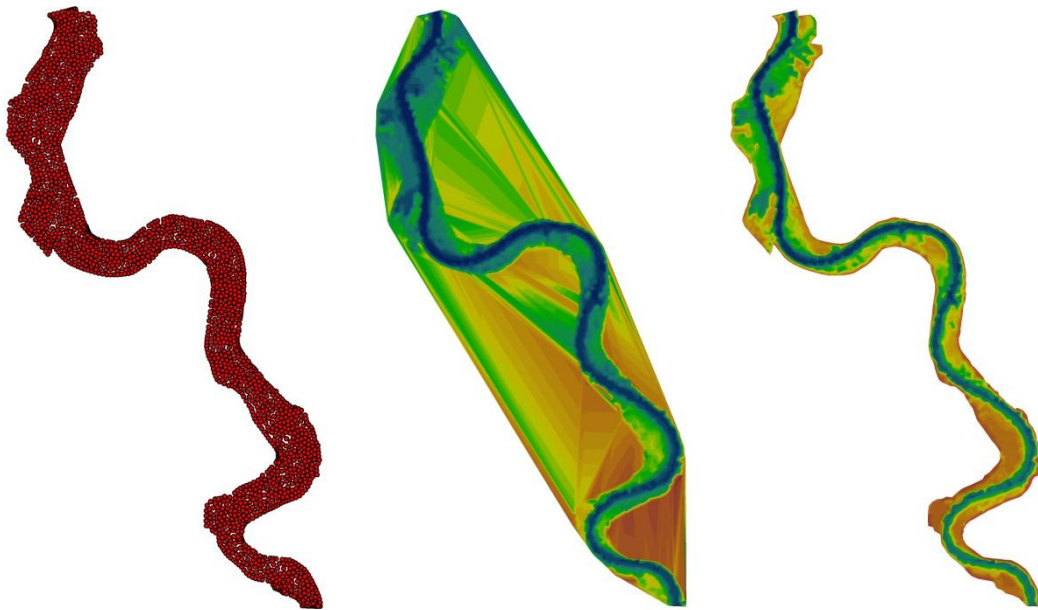


Figure 10: Creation of TINs from mesh nodes generated in the MZMG

For each TIN the volume enclosed by the surface from the zero plane was calculated. The results are presented in the following diagram and table.

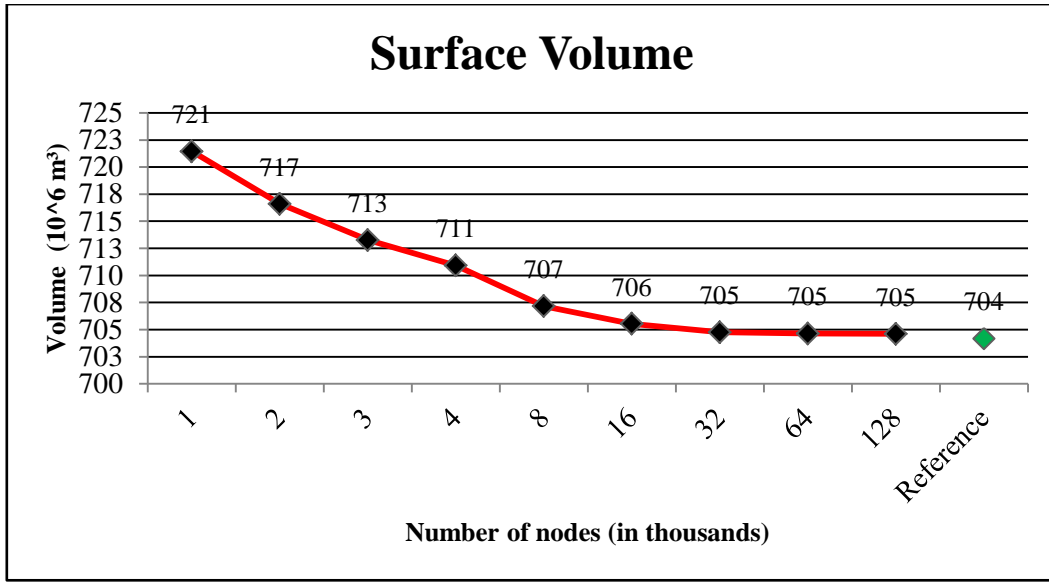


Figure 11: Diagram of the surface volume enclosed by TINs versus the number of nodes used to create these TINs, compared to the benchmark TIN (Reference)

The diagram shows that the surface volume decreases towards the reference volume with increasing number of nodes. This implies that with low mesh resolutions surface elevations are generally overestimated, and hence, the volume enclosed by the river channel including the floodplains is underestimated. This in turn indicates that with low mesh resolutions water levels are predicted too high. The following table shows the computed volumes, the absolute error and the relative error of the different meshes compared to the benchmark TIN.

	Volume (m ³)	Absolute Error (m ³)	Relative Error %
1	721,446,132	17,272,711	2.45
2	716,597,406	12,423,984	1.76
3	713,262,334	9,088,912	1.29
4	710,914,960	6,741,538	0.96
8	707,168,510	2,995,088	0.42
16	705,533,615	1,360,193	0.19
32	704,754,681	581,259	0.08
64	704,642,479	469,057	0.07
128	704,607,700	434,278	0.06
Benchmark	704,173,422	0	0

Table 2: Comparison of the volume enclosed by TINs with respect to the number of nodes used to create these TINs

However, the volumetric evaluation provides only a rough indication for a suitable mesh resolution. Particularly, it does not provide information on the influence of the mesh

resolution on the hydraulic performance of the model. Hence, for each mesh a simulation was run to determine the impact of the mesh resolution on the accuracy of the simulation results.

For this, a simulation file had to be set up. This included the creation of time series for the open boundaries based on the selected flood event, the definition of suitable initial conditions and the specification of different simulation parameters.

8. Set up of the Simulation File

8.1 Time Specification

The time step interval for numerical hydrodynamic computations should generally be selected according to degree of the temporal variation of the simulated event, e.g. for the simulation of a rapidly developing flood wave, a relatively small time step is necessary. Optimally the interval should be decreased to a length at which simulation results remain unaffected. Time step interval independent results can be achieved during a calibration process. For the stability of explicit numerical schemes it is furthermore important to ensure a CFL number below one. Hence, the time step interval should also be selected according to the smallest element and the maximum flow velocity (DHI 2007).

In M21fm the simulation period is specified by defining a start date, a total number of time steps and a time step interval. The time step interval, which defines the minimum frequency for which simulation results can be obtained, is set to 30 seconds. This results in an overall number of 63360 time steps for the entire simulated flood event.

M21fm uses a dynamic internal time step which is determined to ensure the stability of the numerical scheme, and which is synchronized with the user defined time step. The variable time step particularly secures that the CFL number is lower than a user defined critical value in all nodes of the computational grid. The internal time step can be restricted by defining a maximum and minimum time step. The first is set to 30 seconds, and the latter is specified to be 0.01 seconds.

8.2 Solution Technique

The computation time and the accuracy of the calculations within M21fm can be controlled by choosing between a first order scheme and a higher order scheme for both the integration

of time and the spatial discretization. The higher order scheme generally produces significantly more accurate results, but proceeds much slower than the lower order scheme. The time required for computation is increased by a factor of two when using a higher order scheme either for the time integration or for the spatial discretization. Using a higher order scheme in both cases will increase the computing time by a factor of four. The application of a lower order scheme is only recommended in cases where the hydrodynamic processes are mainly governed by diffusion (DHI 2007). Since flow within a river is predominately influenced by convective processes, a higher order scheme is used for the case study of this thesis (Habersack et al. 2007).

For the CFL critical number a value of 0.8 is specified to guarantee numerical stability throughout the simulation.

8.3 Density

As a fluid is assumed to be incompressible in the SWEs, density is only dependent on temperature and salinity. M21fm allows the inclusion of density variations with temperature or salinity by solving their transport equations. However, the effects of temperature are not considered in the case study, and thus a barotropic density was specified.

8.4 Eddy viscosity

As it is generally not yet practical to use computational grids fine enough to resolve the whole range of turbulences, NHMs of any dimension need to be supplemented by turbulence models to account for the sub-grid turbulent fluctuations. M21fm applies an eddy viscosity concept, which can be specified as a constant eddy formulation or a Smagorinsky formulation.

For the case study the Smagorinsky formulation was applied with a default spatially constant Smagorinsky coefficient of 0.28. Furthermore, the default maximum ($1 * 10^{10} m^2/s$) and minimum ($1.8 * 10^{-6} m^2/s$) values of for the eddy viscosity were used.

8.5 Roughness Coefficient

M21fm uses a quadratic friction law to define the bottom shear stress (τ_b):

$$\tau_b = C_f \rho \bar{U}^2 \tag{6}$$

where ρ is the density of the water and \bar{U} is the depth averaged velocity. The drag coefficient C_f can be specified as either a Manning number (M)¹, or a Chezy number (DHI 2007). For the case study of this thesis the M number was used:

$$C_f = \frac{g}{(Mh^{\frac{1}{6}})^2} \quad (7)$$

where h is the total water depth and g is the gravitational acceleration. Hence, a higher M value results in a lower bed resistance. In M21fm the M number can be defined as either spatially constant or varying within the computational domain (DHI 2007). Optimally, for a 2-D river-floodplain model the roughness coefficient should be spatially varying in the domain according to the type of land use and vegetation. This would require the development of a data file which describes the spatial distribution of the coefficient. These roughness coefficient maps are commonly derived from on-site field inspections, photo documentations, or remotely sensed land cover maps together with the use of lookup tables (Habersack et al. 2007; Straatsma and Huthoff 2011). However, due to the lack of such data a constant roughness coefficient was applied for the entire domain. Initially an M coefficient of $32 \frac{m^{1/3}}{s}$ was used which is the recommended value by DHI in case no data is available (DHI, 2007). The roughness coefficient was then optimized during a calibration process and a coefficient of 40 and 32 for the main channel and the floodplains respectively was found to be the most suitable one.

8.6 Specification of the Boundary Conditions

For the specification of the boundary conditions hourly water levels and discharge values from the measuring stations at Ruhort and Wesel were available. The data was obtained from the Bundesanstalt für Gewässerkunde (BFG). The stream gauge in Wesel is located at the Rhine kilometer 814.000 km and water-levels are measured from the gauge zero which is defined at 11.196 above NN². The stream gauge in Ruhrort is found at river kilometer 780.80 and water levels are measured from 16.09 m above NN (WSV 2012).

¹ Note: Other sources use M to refer to the Strickler coefficient and n to refer to the Manning coefficient, where n is defined as the inverse of M . For this thesis, the terminology used by DHI will be adopted and M will be used to refer to the Manning number.

² The standard reference zero for measuring heights used in Germany until 1992.



Figure 12: Pegel Ruhrort (Source: BFG, 2012)

Stream gauge	Wesel	Ruhrort
River kilometer	814.00 km	780. 80 km
Coordinates	Not available	(2550630, 5702560)
Gauge zero	NN +11.196 m	NN+ 16,088 m

Table 3: Information about the stream gauges in Wesel and Ruhrort

The selected simulation period extends from the 22nd of January to the 13th of February 1995. In this way, the main flood event is covered while starting from a point where discharge and water levels are close to the average observed values.

For the land boundary of the model a full slip boundary condition was used, which implies that the normal velocity component of the flow is forced to zero while the tangential flow velocity component is non-zero. The upstream boundary was specified with hourly discharge values and the downstream boundary with hourly water surface levels. The water levels were given relative to the gauge zero defined at 11.196 m above NN. Since the heights of the topographic data used in the model were given with respect to NN, the difference between the two reference zeros had to be added to the water level values. The time series for both boundary conditions were created with the MIKE Zero times series editor.

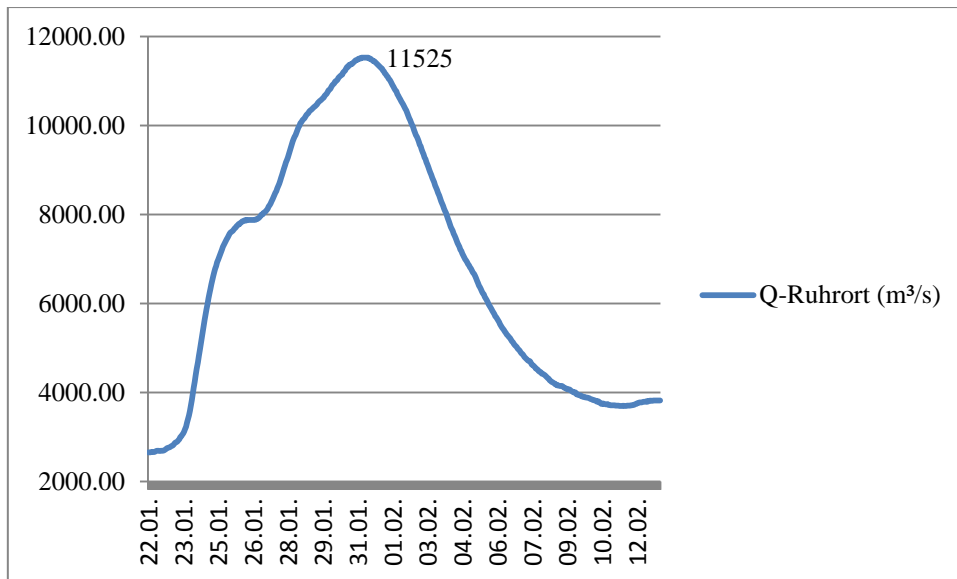


Figure 13: Specified Q at the upstream boundary in Ruhrort

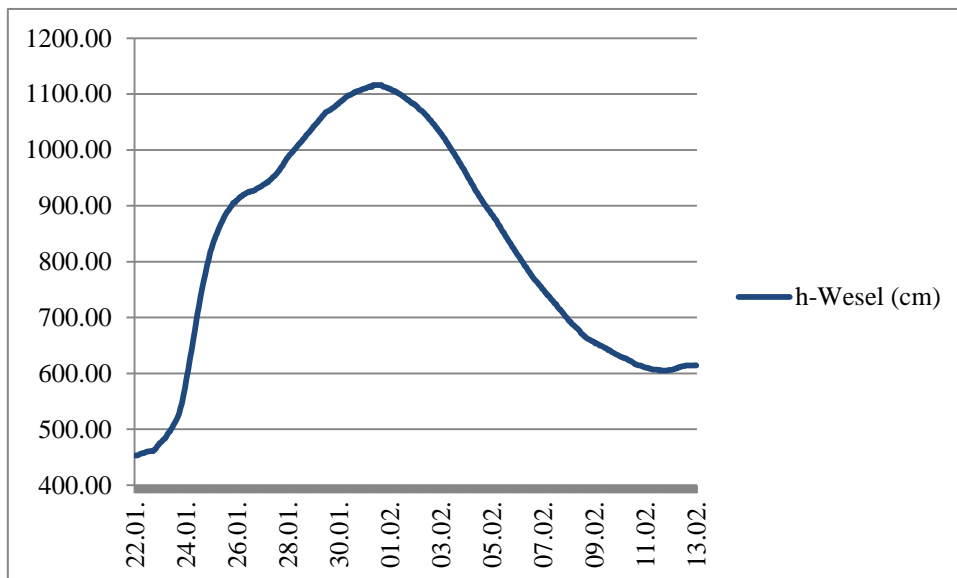


Figure 14: Specified water levels at the downstream boundary in Wesel relative to the gauge zero

For the treatment of the moving boundaries, the flood and dry facility of M21fm was enabled with the following default values:

Drying depth:	Wetting depth:	Flooding depth:
$h_{dry} = 0.005 \text{ m}$	$h_{wet} = 0.1 \text{ m}$	$h_{flood} = 0.05 \text{ m}$

As described earlier, activating the flood and dry facility has the following consequences (DHI 2007):

- If $h > h_{wet} \rightarrow$ both the mass fluxes and the momentum fluxes are computed

- If $h_{dry} < h < h_{wet}$ \rightarrow momentum fluxes are set to zero and only the mass fluxes are computed
- If $h < h_{dry}$ \rightarrow element is removed from the calculation and only re-introduced once $h > h_{flood}$ holds true

8.7 Initial Conditions

At first, a constant initial water level was applied for the entire domain. However, due to the difference in bed elevation between the upper and lower end of the model, this did not allow to have physically reasonable initial conditions at both boundaries at the same time. Therefore, a spatially varying water level was applied to account for the bed slope, and hence to achieve a matching with the specified boundary conditions (Figure 15).

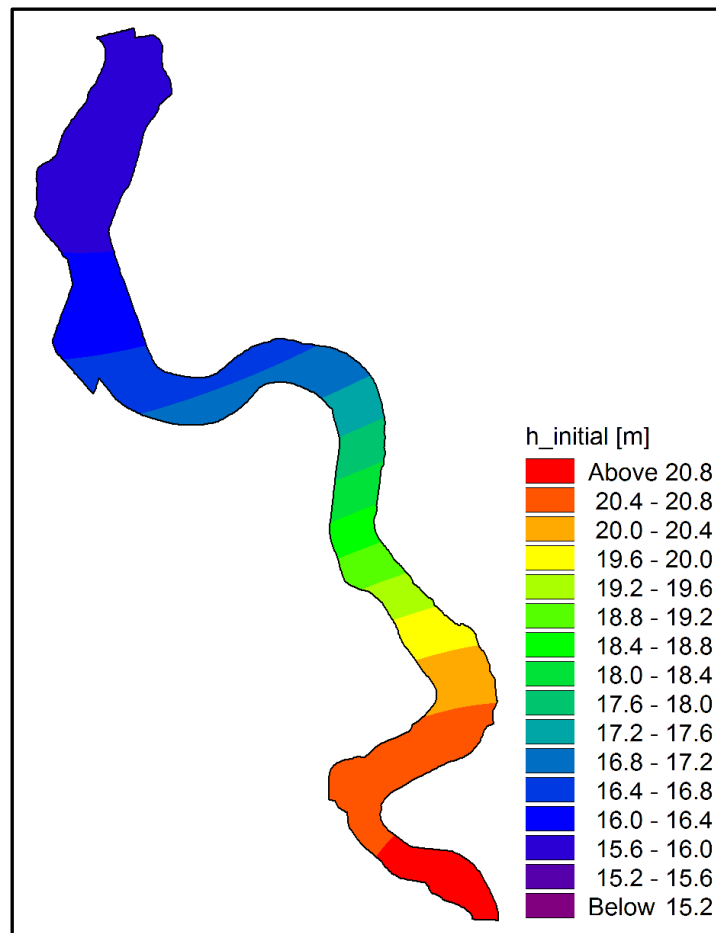


Figure 15: Spatially varying water levels used as initial conditions

The initial conditions were created with the Mike Zero Data Manager, by assigning the measured water levels from Ruhrort and Wesel of one hour before the start of the simulation period to the corresponding mesh elements, and by determining the values between them through interpolation. The file had to be created for each of the used meshes.

9. Hydraulic Performance for different Mesh Resolutions

In order to identify a suitable mesh resolution for the river model the specified simulation was run with different meshes containing a total amount of 1,000 to 16,000 nodes. As the time required for completing the simulation of the 16,000 nodes mesh was already more than two days, meshes of higher resolution were not tested.

The hydraulic performance of the different meshes was evaluated by comparing the calculated discharge values and water levels with the corresponding measured values at the downstream- and at the upstream boundary respectively. For this, two line series perpendicular to the river channel were specified as simulation output: one at the downstream boundary for recording a time series of discharge values, and one at the upstream boundary for recording a time series of water levels. The agreement with the measured values was then assessed by means of graphical visualization, absolute and relative errors³ and the average absolute relative error (AARE)⁴. Other statistical methods will not be considered in this thesis, but the interested reader is referred to the work of Green and Stephenson (1986), which provides a discussion about different goodness-of-fit criteria for hydrographs, or Krause et al. (2005) who investigated nine methods for assessing a models performance in reproducing observed values. The AARE is used here since it provides a simple and unambiguous way of indicating a models average inaccuracy (Willmott and Matsuura 2005).

9.1 Results

9.1.1 Discharge at Wesel

Comparison of the different hydrographs reveals that the simulated discharge values of the model exhibits a low sensitivity for mesh resolution. The only large difference in the

³The error (E) in this thesis is calculated as the difference between the observed and the calculated value. Hence, the relative error (E_{rel}) is calculated as follows: $E_{rel} = \frac{x_{obs} - x_{cal}}{x_{obs}} \times 100$

⁴ The AARE is calculated as: $AARE = \frac{1}{n} \sum_{i=1}^n |E_{rel,i}|$

predicted values occurs at the beginning of the simulation, where the time required for the model to converge toward the measured values generally decreases with increasing number of nodes. The mesh with 1,000 nodes requires approximately 13 hours to “warm up”, whereas the mesh with 16,000 nodes produces realistic values already after 6 hours⁵. However, the initial phase of the simulation (i.e. the first 13 hours) is not relevant considering the total duration of simulated event and will hence be neglected in the further presentation of the results.

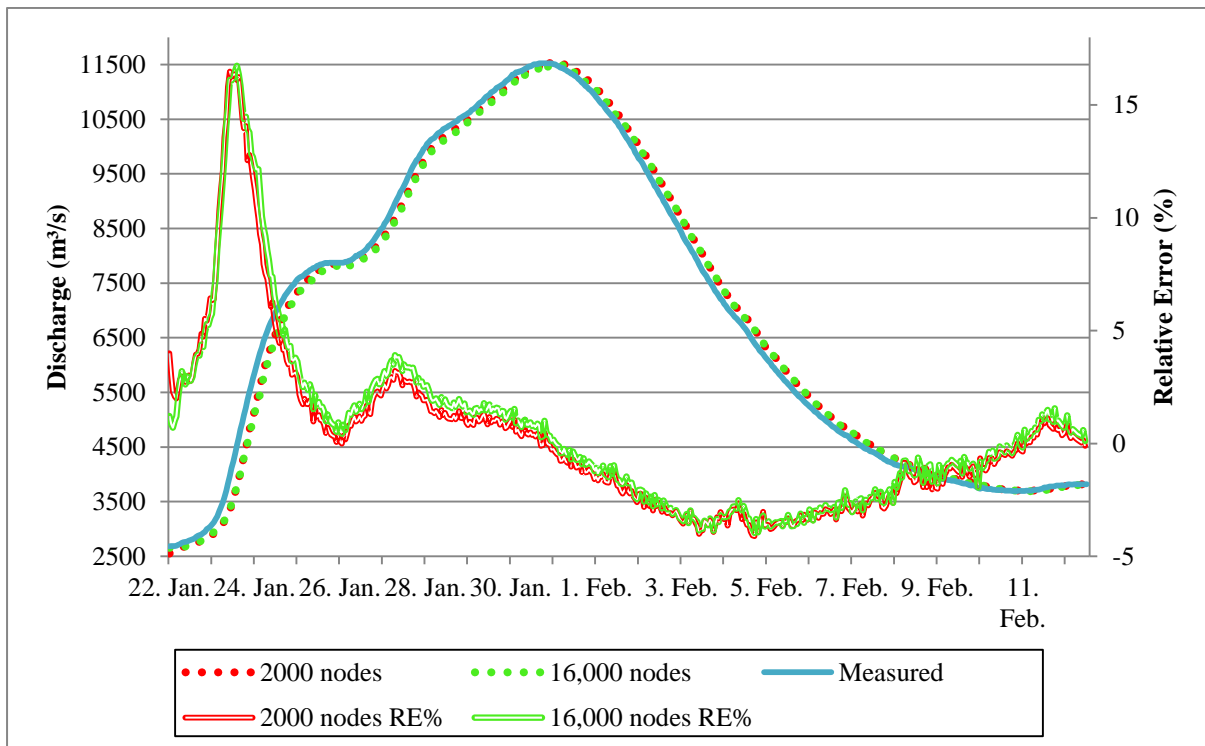


Figure 16: Measured and calculated hydrographs at Wesel and corresponding relative percentage error (RE%) for 2,000 and 16,000 nodes

The performance in matching the observed values was found to be almost the same for each of the used meshes, indicating a low correlation between mesh resolution and accuracy in reproducing discharge values. However, the discrepancies between observed and measured data tend to be slightly higher for meshes of higher resolution. Independent of the mesh resolution used, the model tends to under-estimate the flow rate prior to the occurrence of the flood peak, and conversely over-estimates the flow rate at the recession limb. Figure 16 displays the observed and the predicted hydrographs at Wesel and the corresponding relative percentage errors (RE%) representatively for the mesh of 2,000 and 16,000 nodes.

⁵ This conclusion was based on the time required for the model produce results with a relative error of less than 2.5%

Generally, a good agreement with the observed hydrograph is achieved in all cases with the exception of significant inaccuracies during the second, third and beginning of the fourth day of the simulation, where relative errors of up to 16 % are reached. Apart from this period the maximum relative error is less than 5 % for all used meshes. The AARE ranges between 2.4 and 2.7 %, and slightly increases with increasing mesh resolution (Table 4: AARE). Moreover, as can be seen by the percent error in peak (PEP) in Table 4, for all meshes the magnitude of the flood peak is predicted relatively precisely. However, in all cases the peak discharge is estimated two hours later than the timing of the observed peak.

Table 4 shows furthermore the required computational time for of the used mesh resolutions. As expected the required computational time increases with the number of nodes used. Thus, considering only the performance of the model in calculating discharge values it would seem reasonable to select a relatively coarse mesh for further investigations.

Nodes	AARE(%): Q		
	Wesel	PEP	Time (h)
1000	2.355	-0.60986	0.9
2000	2.609	-0.11097	2.0
3000	2.619	-0.15349	3.2
4000	2.697	0.879007	6.3
8000	2.700	0.041734	9.6
16000	2.716	0.273394	26.3

Table 4: AARE (%) for discharge, PEP and the required computational time for different mesh resolutions

9.1.2 Water levels at Ruhrort

Compared to the calculated discharge values the model exhibits a much higher sensitivity for mesh resolution in the prediction of water levels. For all applied meshes, h-values are systematically over-estimated, but the agreement with the observed values strongly increases with increasing resolution (Figure 17, Figure 18 and Table 5).

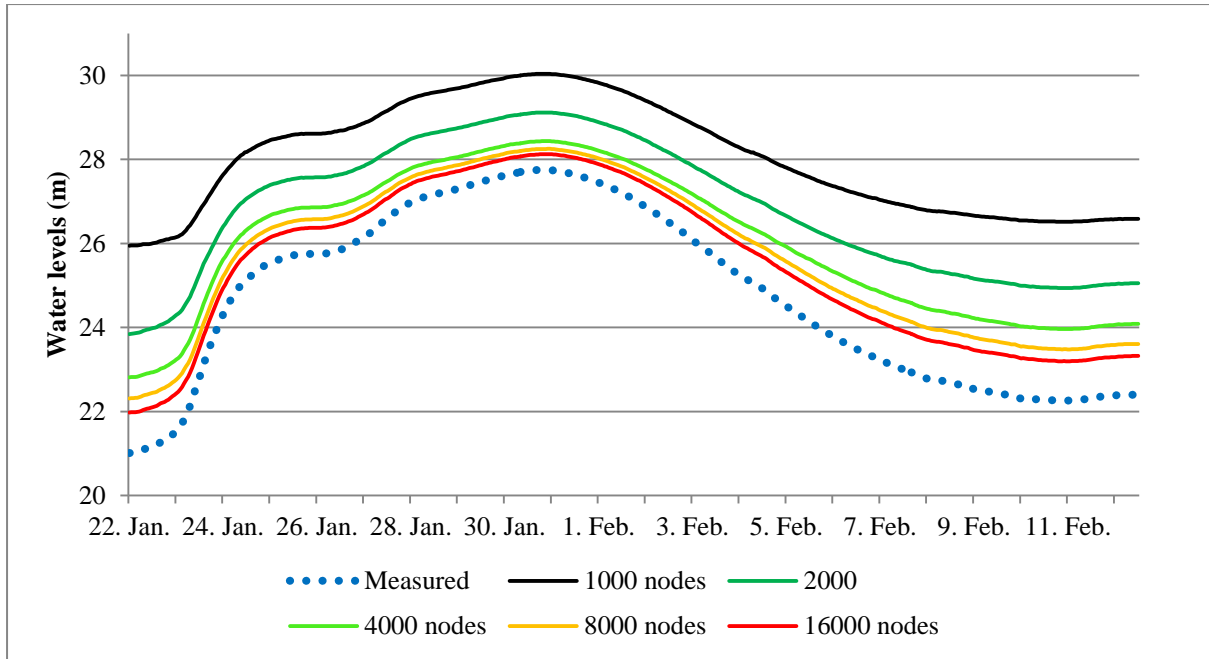


Figure 17: Comparison of the observed and calculated water levels at Ruhrort for different mesh resolutions

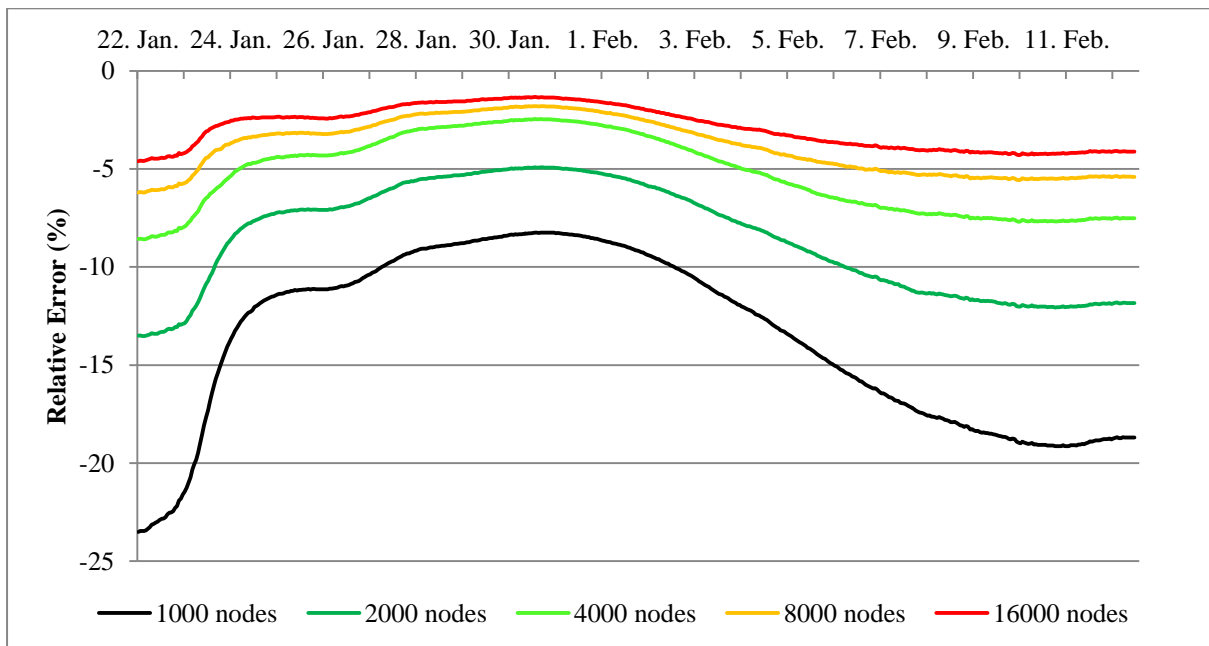


Figure 18: Comparison of the relative errors in matching the observed water levels for different mesh resolutions

The above diagrams display that the model particularly underperforms during the recession of the flood. Even with the mesh of 16,000 nodes, water levels are predicted constantly about 1 m too high throughout the entire last week of the simulation period.

Nodes	AARE(%): h Ruhort	Absolute error range (m)	Time (h)
1000	13.604	(-4.94)—(-2.89)	0.9
2000	8.531	(-2.84)—(-1.36)	2.0
3000	6.391	(-1.54)—(-0.96)	3.2
4000	5.241	(-1.81)—(-0.68)	6.3
8000	3.833	(-1.30)—(-0.50)	9.6
16000	2.892	(-0.97)—(-0.37)	26.3

Table 5: AARE and the absolute error range in the prediction of water levels as well as the required computational time for different mesh resolutions

9.2 Discussion and Conclusion

In summary, the mesh resolution was identified to have a low influence on calculated discharge values and a strong influence on the prediction of water levels. An acceptable matching with observed q-values was achieved independent of mesh resolution except for large discrepancies during the third and fourth day of the simulation. Moreover, by comparing hydrographs obtained in the middle of the river section, it was proved that the low dependence of predicted discharge values on mesh resolution is not caused by the influenced of the downstream boundary conditions.

On the other hand, relatively accurate water levels could only be obtained with meshes of high resolution. However, even a mesh containing 16,000 nodes resulted in considerable over-estimations of the h-values. This indicates the necessity of further mesh improvements through e.g. local mesh refinements or the addition of breaklines and a parameter optimization on the base of a calibration process.

From the above observation it is clear that for optimum results a mesh of 16,000 or more nodes should be applied. However, considering the required time to run the simulation, the mesh containing 8000 nodes seemed to be a better compromise between accuracy and computation speed for the purpose of this study. Moreover, the reported inaccuracies of the model may also be related to an incorrect selection of the simulation parameters. Particularly the systematically over-estimated water levels indicate that the bed resistance has to be decreased. It thus was concluded that before unnecessarily high mesh resolution are used

other means of increasing the simulation accuracy should be tried. This was done through mesh improvements by creating a locally refined mesh for the river channel and by adding breaklines for the river banks and the thalweg, as well as by an optimization of the roughness coefficient through calibration.

10. Measures to Improve the Grid

10.1 Creation of an Internal Polygon for the River Channel

As a first measure to improve the grid, an internal polygon enclosing the river channel was created to allow for a separate and finer triangulation within the channel. Furthermore, by placing connected nodes along the river it is ensured that the z-values and the linear shape of the river banks are preserved during interpolation and triangulation respectively. Hence, the two long sides of the polygon in served as breaklines which forced triangle edges to be aligned along the river bank. Moreover, the created polygon also facilitated the application of a separate roughness coefficient for the river channel and the floodplains.

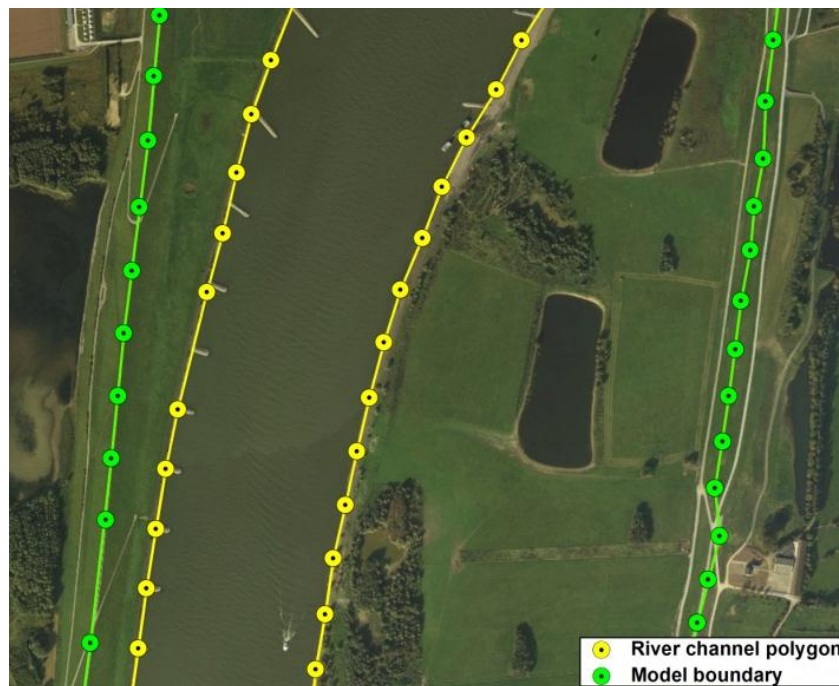


Figure 19: Internal polygon for the river channel (Source: Bing Maps Aerial, 2012)

The internal polygon was constructed in ArcMap 10 by tracing the river banks on a satellite image provided by Bing Maps Aerial (Figure 19). The created vector data was then imported as an ASCII file into the MZMG. In the MZMG the internal polygon was used to create a

refined mesh within the river channel by specifying a maximum element area which is about half of the size of the maximum element area for the mesh on the floodplains.

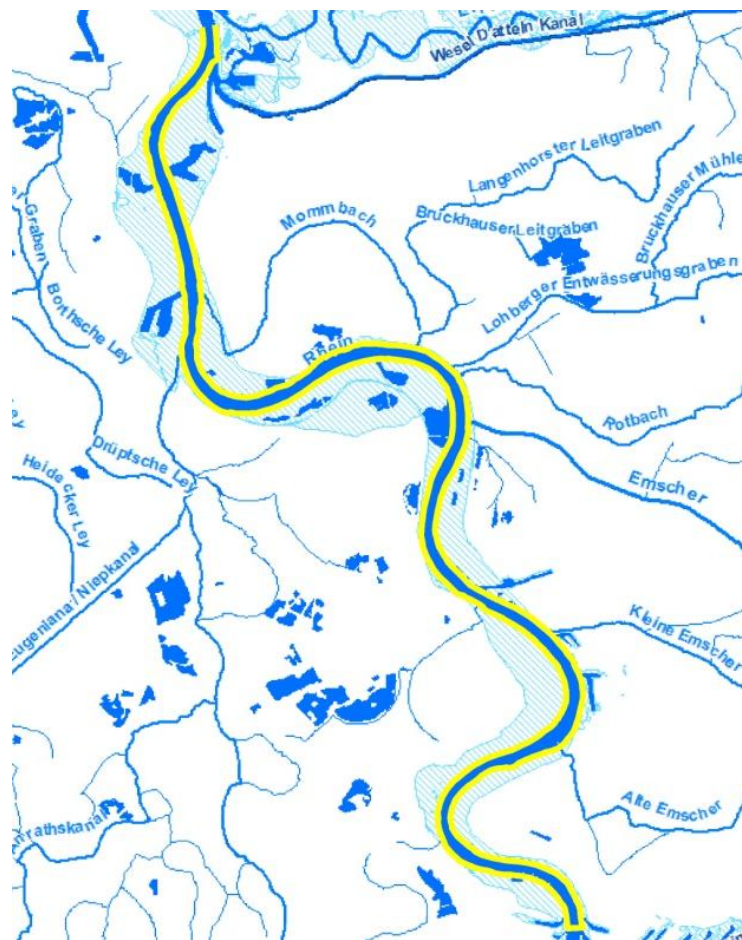


Figure 20: Internal polygon on a map showing the main river channel (Source: Geoserver NRW 2012)

10.2 Creation of the Thalweg

Another measure to improve the geometrical representation of the channel was to create a line of connected nodes along the deepest point at each cross section. This line, which is commonly referred to as thalweg, ensures that the available bathymetry points of lowest elevation will be preserved in the model during interpolation. The points were identified within MS Excel through sorting, and were then imported as connected nodes into the MZMG. Figure 21 shows that the thalweg results in an improved representation of the river channel.

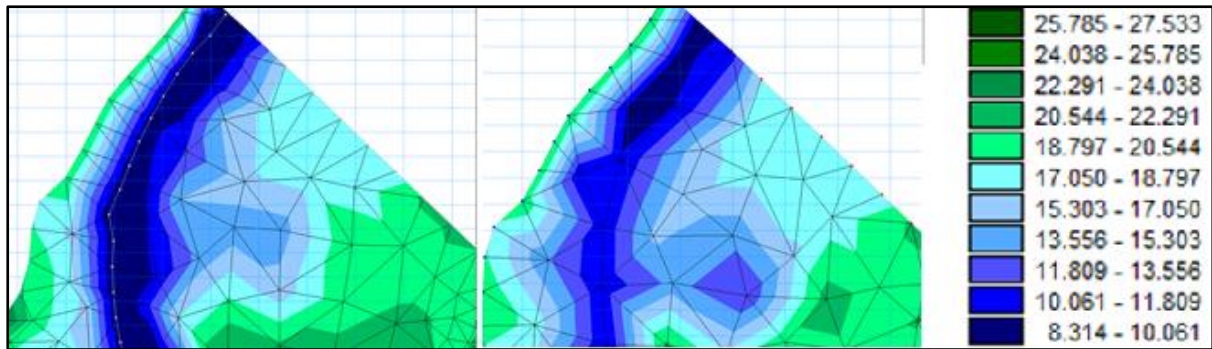


Figure 21: Mesh with (left) and without the created thalweg feature

10.3 Results of the Mesh Improvements

The effect of the described mesh modifications on the models computation accuracy were evaluated by comparing the performance of the following four meshes in matching the observed water levels and discharge values:

- 8000 nodes without any modifications (8nm)
- 16000 nodes without any modifications (16nm)
- 8000 nodes with internal polygon and river channel refinement (8ip)
- Mesh 8ip plus the created thalweg (8ip_th)

With respect to the calculated discharge values no significant difference between the different meshes was observed, whereas for water levels both mesh modifications resulted in an improved matching with the observed values compared to the mesh without modifications (Table 6 and Figure 22). The mesh containing both modifications even showed a consistently better performance compared to the mesh of 16,000 nodes. However, both the channel refinement and thalweg considerably increased the required computational time. As a consequence, the simulation duration for the mesh containing 8,000 nodes and both mesh improvements is approximately equal to simulation duration of the unmodified 16,000 nodes mesh.

Mesh	AAER (%) q	AAER (%) h	Time (h)
8nm	2.700	3.833	9.6
8ip	2.734	2.978	20.1
8ip_th	2.728	2.715	26.0
16nm	2.716	2.892	26.3

Table 6: Absolute average relative error (AAER) for discharge (q) and water levels (h) and the required computational time for different meshes

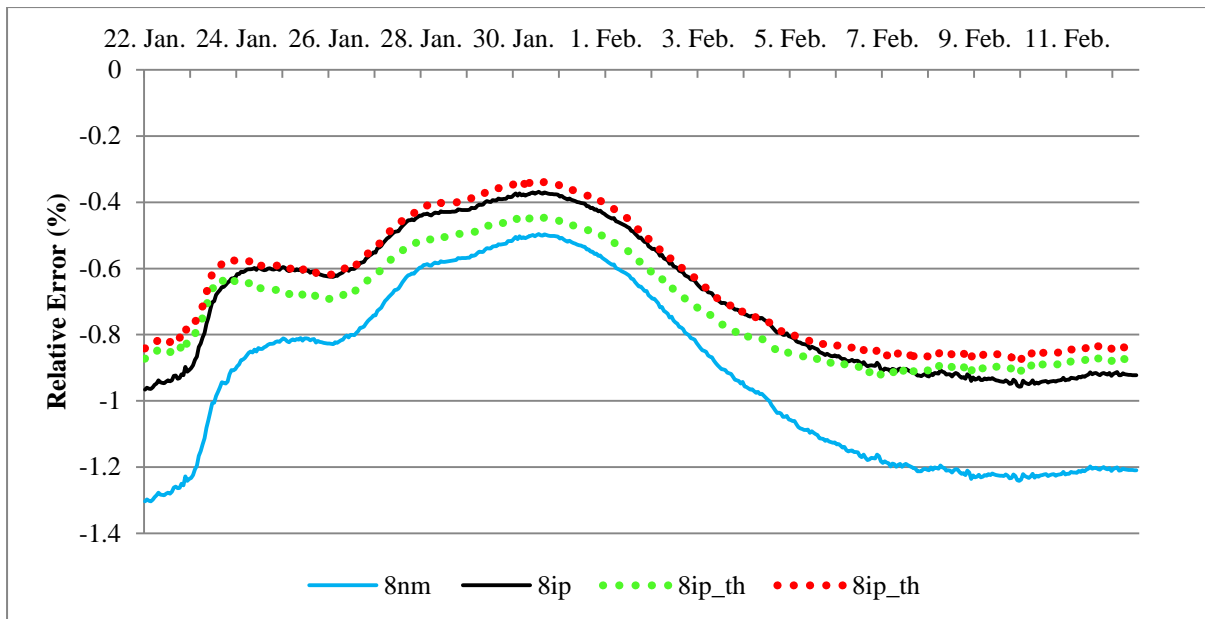


Figure 22: Comparison of the relative error (%) in the calculation of water levels for different meshes

10.4 Conclusion

It was shown that both a mesh refinement within the main channel and the addition of breaklines increase the models accuracy for a constant number of mesh nodes. The drawbacks of these measures are increased computational times as both the refinement and the additional nodes of the breaklines decrease the size of mesh elements.

The mesh of 8,000 nodes including a refinement of the main channel and breaklines for the river bank and the thalweg was identified to provide the best-fit with the observed data from the tested meshes. It will therefore be used for the case study of this thesis. Despite of some improvements, water levels were still systematically over-estimated, therefore a calibration was conducted to determine a more suitable roughness coefficient.

11. Calibration

11.1 Theoretical Background

Calibration is the process of varying parameters until a suitable match of the simulation results with the observed data is achieved. Hence, it is the identification of the optimal set of parameters. However, it has to be considered that the optimum parameters for a specific event may not be the optimum parameters for a different event, particularly if the two events differ strongly in magnitude (Horritt and Bates 2002). Generally, calibration should only be carried out within realistic parameter ranges as otherwise the predictive ability of the model can be

greatly reduced, particularly for flow variables which were not subject to calibration (e.g. flow velocities). Data commonly used for calibration include measured water levels, discharge values or flow velocities (Habersack et al. 2007). For flood inundation models, also remotely sensed maps of flood inundation extend can be used. The combined use of hydrometric and inundation extend data has been demonstrated to be an effective way of discriminating between different models for flood inundation (Horritt and Bates 2002).

Prior to the calibration process a sensitivity analysis can be helpful to obtain trends on how the model results are affected by parameter modifications. Thereby, a faster calibration process can be achieved, and parameters which exert the largest influence on the simulation results can be identified. A sensitivity analysis may also be used for assessing the uncertainties of a model with respect to the selected parameters in case no data for calibration is available (Habersack et al. 2007). For the presented case study this applies for the roughness coefficient of the polder. As no data is available to calibrate this parameter, its selection will be based on an estimate. To evaluate the range of the potential error of this estimate, a sensitivity analysis could provide the necessary information. However, due to time constraints a sensitivity analysis was not performed.

11.2 Calibration of the Roughness Coefficient

A calibration will only be conducted for the roughness coefficient of the river model by using the available observed water levels and discharge values. This can be justified as the roughness coefficient has a strong influence on the water levels, and hence on the occurrence of overbank flow. It has been identified in many flood inundation models as the parameter with the highest sensitivity (Schumann et al. 2007).

The over-estimation of water levels suggests that the flow resistance has to be decreased, which implies that the M coefficient as defined by DHI (i.e. $[\frac{m^{1/3}}{s}]$) has to be increased. Therefore, the M value was increased from initially 32 to 37 and then 40. For comparison, also an M value of 20 was used. As the variation in a spatial constant roughness coefficient improved the simulation results only to a limited degree, a separate coefficient of 40 and 32 two was applied for the river channel and the surrounding floodplains respectively. The spatially varying roughness coefficient was created with the Mike Zero Data Manager by assigning the mentioned coefficients to the corresponding elements in the domain. The

distinction between the river channel and the floodplains was based on the in chapter 10 described internal polygon.

11.3 Results

Increasing the M coefficient resulted in a better agreement of both the calculated discharge values and the calculated water levels with the observed data, whereas using coefficients of lower magnitude resulted in the opposite. The improvements for the discharge predictions were rather small and occurred mainly in the form of a reduction of the previously mentioned peak in discrepancies with the observed data during the second and third day of the simulation period. In other words, using an M coefficient of 40 instead of 32 reduced the maximum error from 17 % to 15 %. Apart from this initial period the calculated discharge values were influenced only to a minor degree by variations in the roughness coefficient. This conclusion is also consistent with the fact that neither the timing, nor the magnitude of the peak discharge was noticeably affected by an increase in the coefficient. Lowering the coefficient on the other hand to 20 delayed the occurrence of the maximum discharge by further 5 hours. Considering the AARE and the maximum relative error, an M value of 40 and the spatially varying value of 40 and 32 resulted in the best agreement with the observed discharge values (Table 6).

$M \left(\frac{m^{1/3}}{s} \right)$	AARE q (%)	AARE h (%)	Max. RE q (%)	Max. RE h (%)
20	3.199	9.957	20.25	11.40
32	2.729	2.713	17.12	4.01
37	2.619	0.992	16.00	2.04
40	2.571	0.760	15.41	1.51
40/32	2.626	0.622	15.54	1.08

Table 7: Absolute average relative error (AARE) and maximum relative error (max. RE) of different Manning coefficients (M) for discharge (q) and water levels (h)

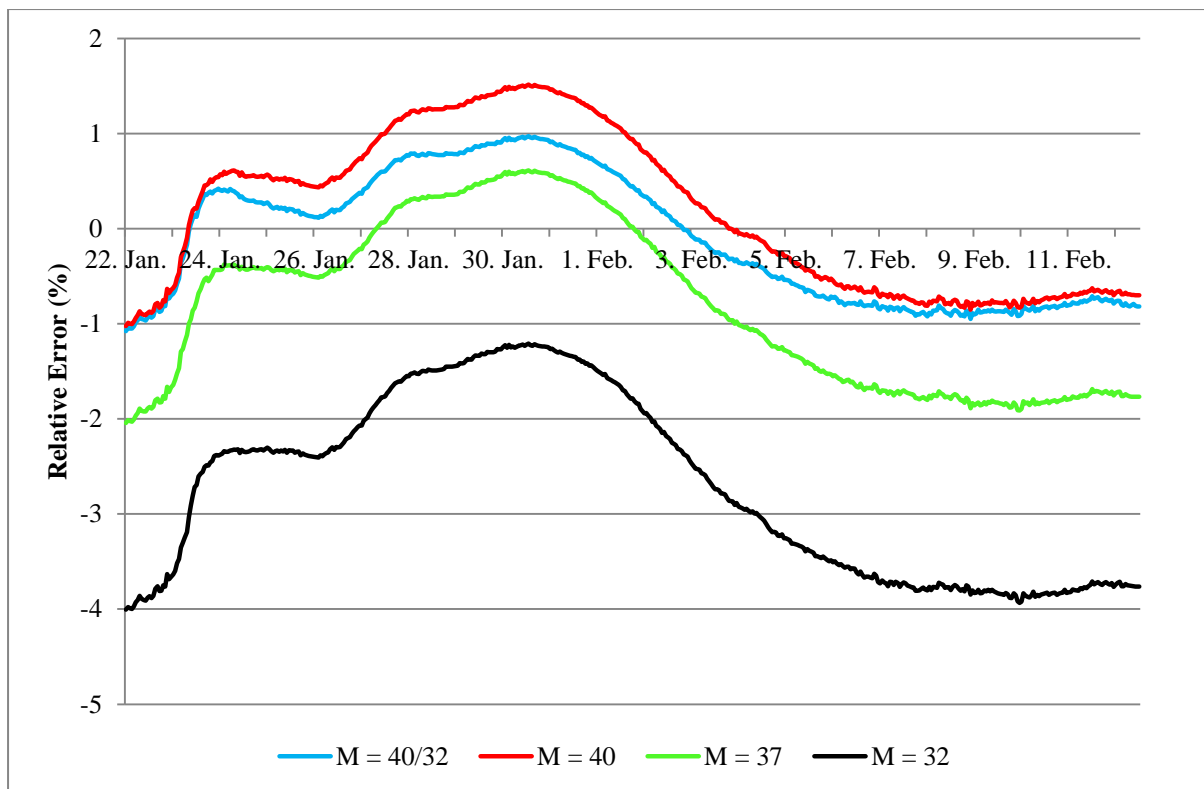


Figure 23: Relative percentage error in the calculation of water levels for different Manning values

Variations in the roughness coefficient showed a relatively large effect on the predicted water levels. Increasing the coefficient resulted in a systematically better agreement with the observed water levels (Figure 23). The best results were achieved with the spatially varying M value which resulted in a reduction of the AARE to 0.62 % which corresponds to roughly 15 cm in absolute terms. Using these M values, the maximum water level is under-estimated by ca. 25 cm.

11.4 Discussion and Conclusion

The model was observed to have a low sensitivity for variations in the roughness coefficient with respect to the calculation of discharge values, and a relatively high sensitivity with respect to the calculation of water levels. The best match with both the observed q- and h-values was achieved with a spatially varying M value of 40 and 32 for the river channel and the floodplains respectively. Using this roughness parameter setting, the model slightly under-estimates water levels for most of the flooding event and over-estimates them during the beginning and the recession of the flood. This suggests that results could be further improved by increasing the resistance for the floodplains and by slightly decreasing the

resistance in the river channel. However due to time constraints a more extensive calibration was not carried out.

Moreover, the large inaccuracies in predicted q -values during the first days of the simulation period could not be reduced to an acceptable degree through calibration of the roughness coefficient. Even with the optimized coefficient, the model under-estimates the discharge by an average of almost 10 % (i.e. ca 426 m³/s) for the entire second and third day of the simulation, which amounts to a share of 25% of the total absolute error. This peak in errors roughly corresponds to the time when the specified inflow first reaches the downstream boundary. Hence, it was assumed that these errors are related to the lack of the specified initial conditions in accounting for flow velocities.

After calibration usually a validation is performed. Validation is the process of assessing the models predictive power for a data set which was not used for calibration. Hence, it is the test to determine whether a model provides reliable results also for other events (Habersack et al. 2007). Due to time constraints a validation was not performed. Hence, the model's accuracy for other boundary conditions than the ones used is uncertain.

12. Generation of the Polder Model

12.1 Introduction to the Modeling Task

The next step was to create a computational mesh of the polder area for which the dike breach will be simulated. This included the definition of the polder boundary, the extraction of topographic points from a DEM and the creation of a continuous surface from these points through triangulation and interpolation. The extracted points should be selected to allow for a realistic representation of the polder topography. Particularly hydraulically significant features such as local peaks and valleys should be included. Subsequently, a suitable amount of nodes have to be identified to properly account for the selected topographic data and to allow the flooding to be simulated with a sufficient resolution. Hence, the quality of the polder model will depend on both the topographic sampling and the mesh resolution.

12.2 Available Data

The available data for the polder consists of a raster based DEM with a cell size of 10 × 10 m. According to Horritt and Bates (2002), for river-floodplain models the grid resolutions should

be between 25 and 100 m, and the vertical accuracy should be better than 25 cm. Furthermore, they showed in a study on the “effects of spatial resolution on a raster-based model for flood flow” that a grid resolution of 50 m proved to be sufficient for allowing detailed predictions of inundation areas (Horritt and Bates 2001).

12.3 Creation of the Polder Boundary

First, the model boundary was defined by creating a polygon surrounding the potential inundation area of the polder. For this, a georeferenced map which shows the spatial extent of a statistically 100-year flood event for a scenario without dikes was delineated by using the editor function of ArcMap 10 (Figure 24). Obviously, the lower boundary of the polder corresponds to the dike which has already been defined for the river model. The “add surface information” tool is then used to add z-values to the created boundary points through interpolation of the DEM.

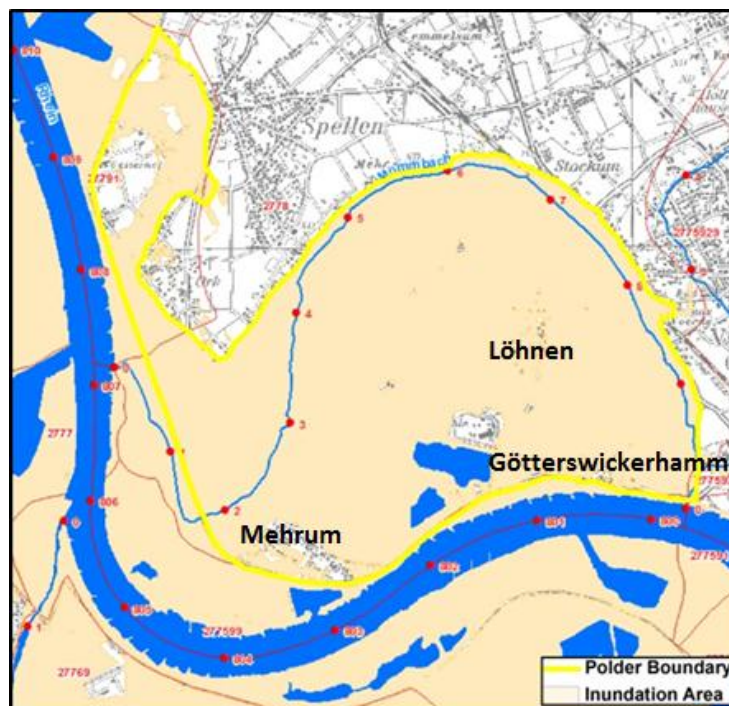


Figure 24: The created polder boundary on a flood inundation map for a scenario without dikes (Source: Geoserver NRW)

The total area enclosed by the polder boundary is approximately 12.86 km², and consists of 232 points which will serve as nodes for the triangulation of the domain. Within this area fall three districts of the city Voerden, namely Mehrum, Löhnen and Götterswickerhamm. The created boundary points are then converted into an ASCII file for application within the MZMG.

12.4 Extraction of 3-D Points from the Polder Area

The next step consisted of extracting single points from the DEM. For this, the DEM is converted into a multipoint feature class, whereby cell centers of the raster file are converted into 3-D points. ArcGIS provides several filtering methods which can be employed to extract only a limited amount of points. However, since the data volume of the complete data set did not pose a problem no filtering method was applied. Hence, each cell of the raster was converted into a point vector resulting in a constant spacing of 10 m between individual points. The clipping tool was then used to delete all points located outside of the study area by employing the previously created polder polygon. From the extracted points an ASCII file was produced which was subsequently imported into the MZMG.

12.5 Determination of a Suitable Mesh Resolution for the Polder

12.5.1 Volumetric Comparison

In order to determine a suitable number of nodes for a sufficient topographic representation of the polder area, a mesh resolution study was conducted. For this, meshes of different resolutions were generated within the MZMG, and a volumetric comparison of TINs created from the associated grid points was done within ArcMap 10. The procedure was similar to the one described earlier. Again, the minimum angle between two lines of a triangular element was specified to be 26 degree. For interpolation of the topographic data onto the mesh, the natural neighbour interpolation routine was applied as it delivered to most accurate results. This conclusion was drawn from a 3-D visualization within the Mike Zero Animator of meshes created with both linear and natural neighbour interpolation. Particularly with respect to the representation of the domain boundary, the natural neighbour method was found to be the better option.

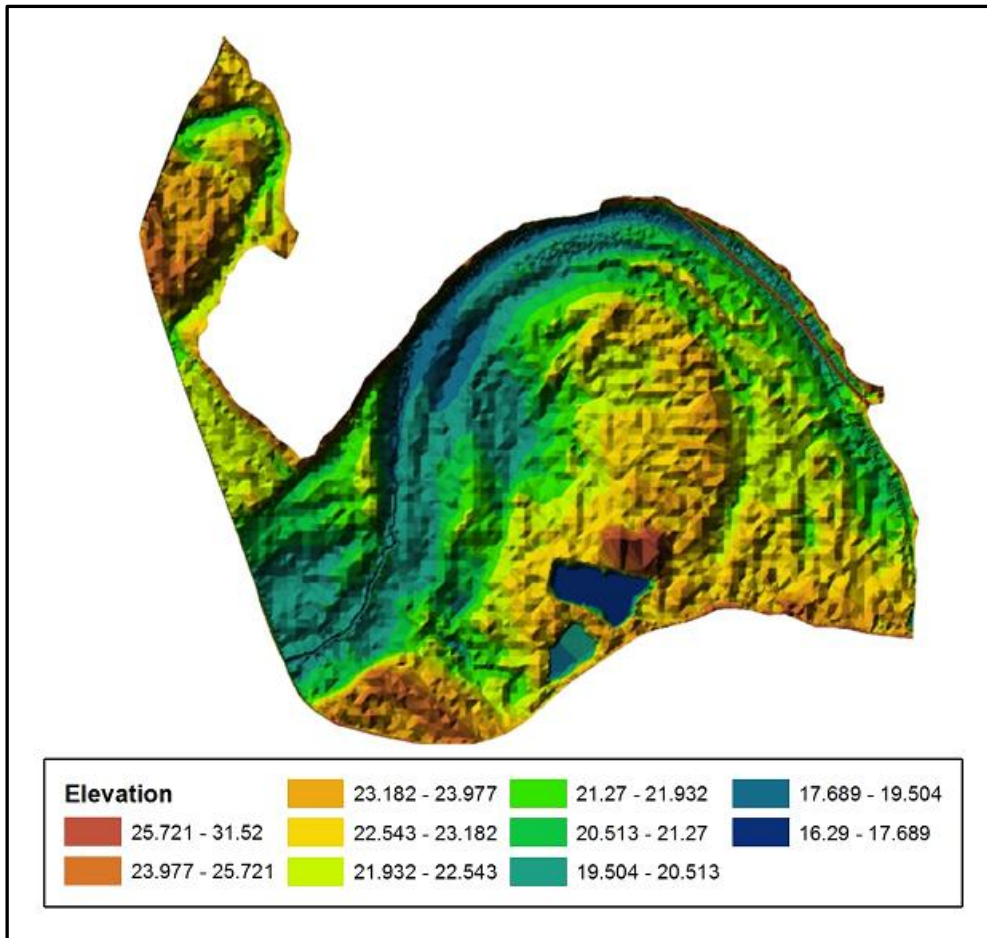


Figure 25: Benchmark TIN of the polder area incorporating to complete available topographic information

The surface volume of each TIN was calculated from a reference plane at 15 m which is below the minimum z-value of the topographic data. The volumes are compared against a benchmark TIN, which was created from a point feature class containing the topographic information of all raster cells from the original DEM (Figure 25). Hence, the benchmark TIN represents the maximum topographic accuracy achievable with the available data.

The results of the volumetric comparison as presented in Figure 26 and Figure 27 clearly show that with decreasing mesh coarseness the volume enclosed by the related TINs decreases toward the benchmark volume. This implies that low mesh resolutions result in an overestimation of the polder surface elevation which would likely result in an underestimation of the predicted flood extend during a hydrodynamic simulation. Nevertheless, it is difficult to identify an optimum mesh resolution from the calculated volumes since the discrepancies in matching the benchmark volume cannot be directly linked to inaccuracies of the vertical surface representation within the model. The spatial distribution of the volumetric errors is not known, and hence their significance for the

simulation of the inundation process cannot be assessed. However, considering the relatively large volumetric difference between the mesh of 3,000 and 4,000 nodes, it seems to be a reasonable conclusion to use at least the latter amount of nodes.

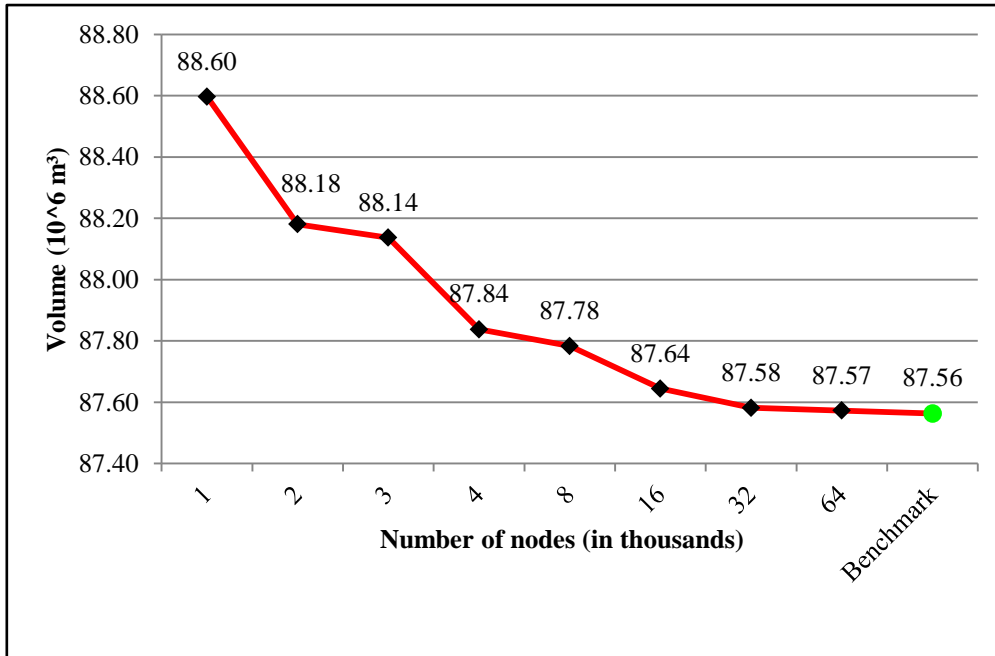


Figure 26: Calculated volumes enclosed by TINs created from nodes which were extracted from meshes of increasing resolution, compared to the volume of a benchmark TIN containing the complete set of available topographic information.

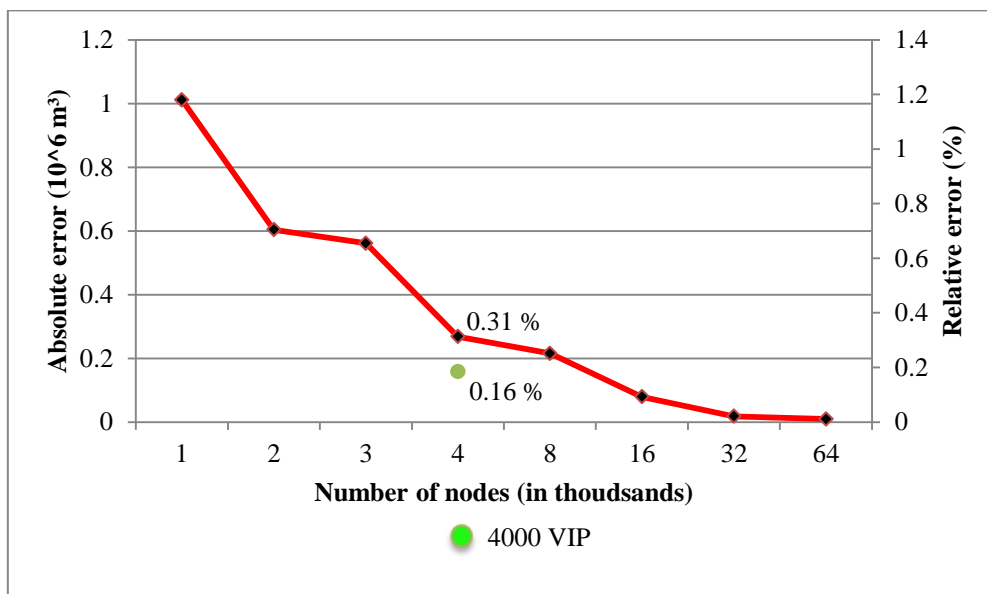


Figure 27: Absolute and relative errors of different mesh resolutions in matching the benchmark volume. The green dot represents a mesh of 4,000 nodes including significant topographic points extracted through the VIP method.

Furthermore, it was attempted to improve the surface representation of the meshes by introducing nodes at topographically significant points. These points were identified and extracted from the DEM by using the Very Important Point (VIP) method which is provided within ArcGIS. This filtering method assesses raster files through a 3x3 roving window, and only extracts the topographically most important ones. According to ESRI (2012), the method is suitable for detecting local peaks and pits, but is however sensitive to noise and insensitive to features larger in size than the used window. The identified 3-D vector points are then imported as an ASCII file into the MZMG where they were converted into unconnected nodes. In this way, the identified points and their z-value will be preserved within the model. Furthermore, in order to avoid the generation of very small triangles, nodes which were closer to each other than 25 meters were removed by applying the mesh generator's "clean data" tool, and nodes located at close distance to the boundary lines were eliminated manually. Thereby, the initially more than 4,000 nodes were reduced to less than 1,300 (Figure 28). From these nodes a mesh of 4,000 nodes was generated, and its volume was calculated in the same way as was done for the other meshes. Figure 27 shows that the insertion of the topographically significant points resulted in a smaller volumetric difference from the benchmark volume.

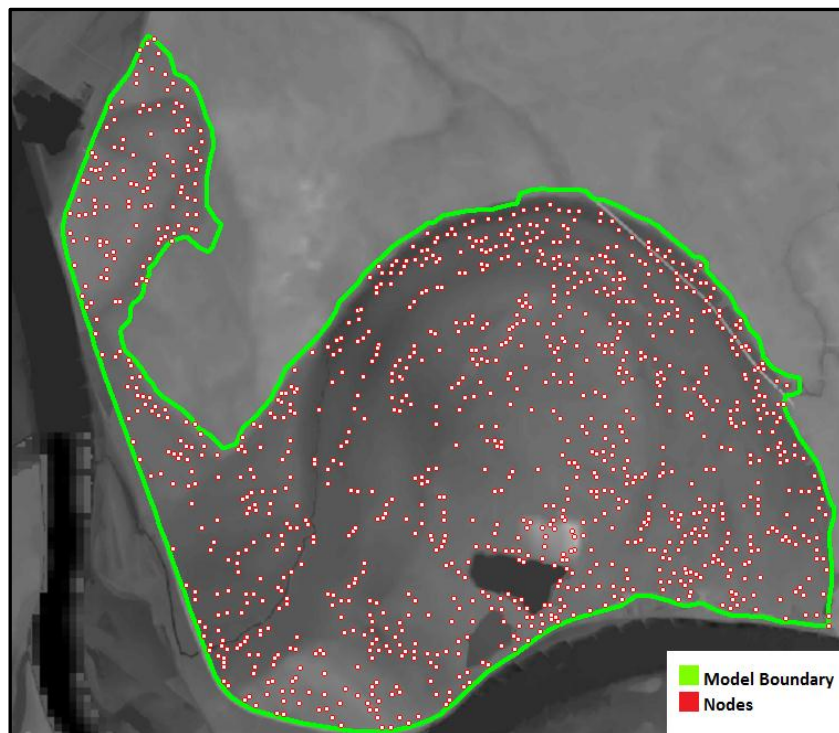


Figure 28: Reduced set of the Very Important Points (VIP) on the DEM

12.5.2 The ArcGIS Tool “Decimate TIN Nodes”

A further option to determine a suitable amount and distribution of nodes for an intended vertical accuracy of a TIN is to use the “decimate TIN nodes” function of ArcMap. This function employs an iterative algorithm to produce a TIN of a reduced subset of nodes from an input TIN within the constraints of a user-defined tolerance for the deviation of the z-values. That is, it is ensured that the difference between the z-value of any node contained in the created TIN and the z-value at the corresponding place of the input TIN is not larger than the specified tolerance (ESRI 2012). The tool also allows specifying the maximum number of nodes used for the creation of the new TIN. Table 8 shows the determined number of nodes from the benchmark TIN for different z-tolerance values.

Having produced a TIN for a certain vertical accuracy, the ArcGIS tool “extract nodes” can then be employed to obtain the complete set of TIN nodes as a vector point file which can then be imported as ASCII file into the mesh generator. However, it has to be considered that due to an irregular distribution of the produced nodes, the MZMG has to add a relatively large number of additional nodes in order to satisfy the smallest allowable angle criteria.

Z-Tolerance (cm)	Number of Nodes
0	133,357
5	28,034
10	17,779
25	9,616
50	6,093
100	5,984
150	2,883
200	2,412

Table 8: Number of nodes for different vertical accuracies

Due to time constraints, the decimate node number approach was not further used. For the final mesh of the polder, a mesh of 4,000 nodes containing the significant points identified through the VIP method was used.

In addition, it would be necessary to evaluate the hydraulic performance of the different meshes by running simulations for each of them, and by comparing the results with observed data. This could potentially be done by comparing the predicted flood extend with flood

extend maps obtained through remote sensing. Using flood extend maps is a common practice for evaluating the performance of hydrodynamic flood models. However, in this case study the predicted flood extend will be strongly influenced by the defined characteristics of the dike breach in terms of its spatial extend. Hence, even if such data was available, its use for assessing the quality of the polder model would be questionable.

13. The Combined Model

Integrating the model of the polder with the model of the river resulted in a total of roughly 12,000 nodes. In order to allow for a separate triangulation of the polder and the river area a polygon marker was introduced at the polder. The roughness coefficient for the polder was specified as an M value of 25 which is recommended by DHI for floodplain applications (DHI 2007b). Certainly this assumption will result in an unknown uncertainty of the predicted flood extend. As mentioned earlier, a sensitivity analysis could be carried out to assess the influence of the roughness coefficient on the spatial development of the flooding.

Initial conditions were created again by interpolating the water levels at Ruhrort and Wesel of one hour before the start of the simulation period throughout the entire domain. The assigned water levels for elements within the polder were then manually reduced to zero again. Moreover, a water level of 18 m was specified at the location of a lake in order to prevent that an unrealistic amount of flood water was stored within the in the model represented basin (Figure 29).

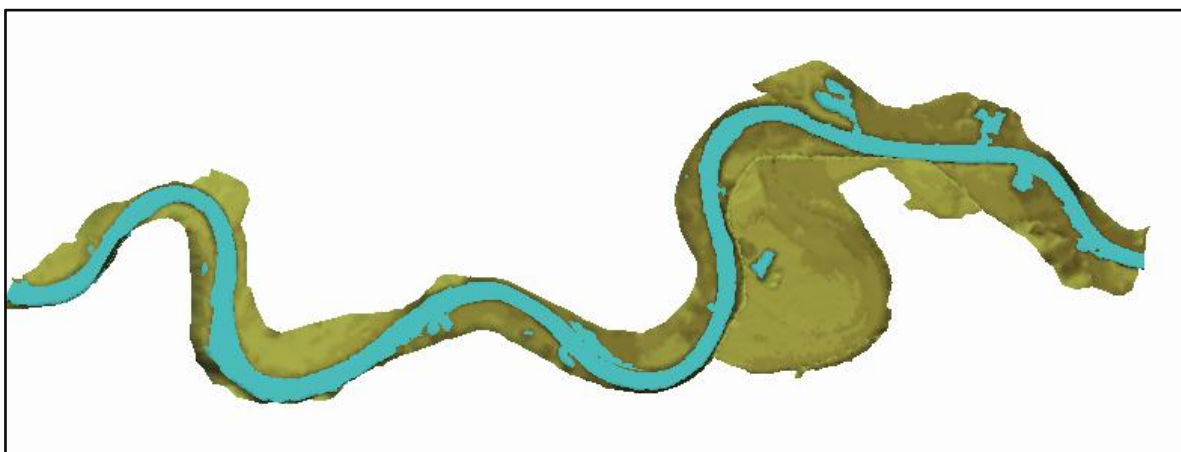


Figure 29: Combined model of the river and the polder including the specified initial water levels

13.1 Dike Breach

The dike breach was created at a location where the river channel is close to the dike by lowering the elevation of the dike over a stretch of 150 m to the ground level (Figure 30). This was done by deleting topographic data along the dike line and by manually modifying the z-values of nodes. Hence, the assumption of a complete collapse of the dike is assumed at the beginning of the simulation period.

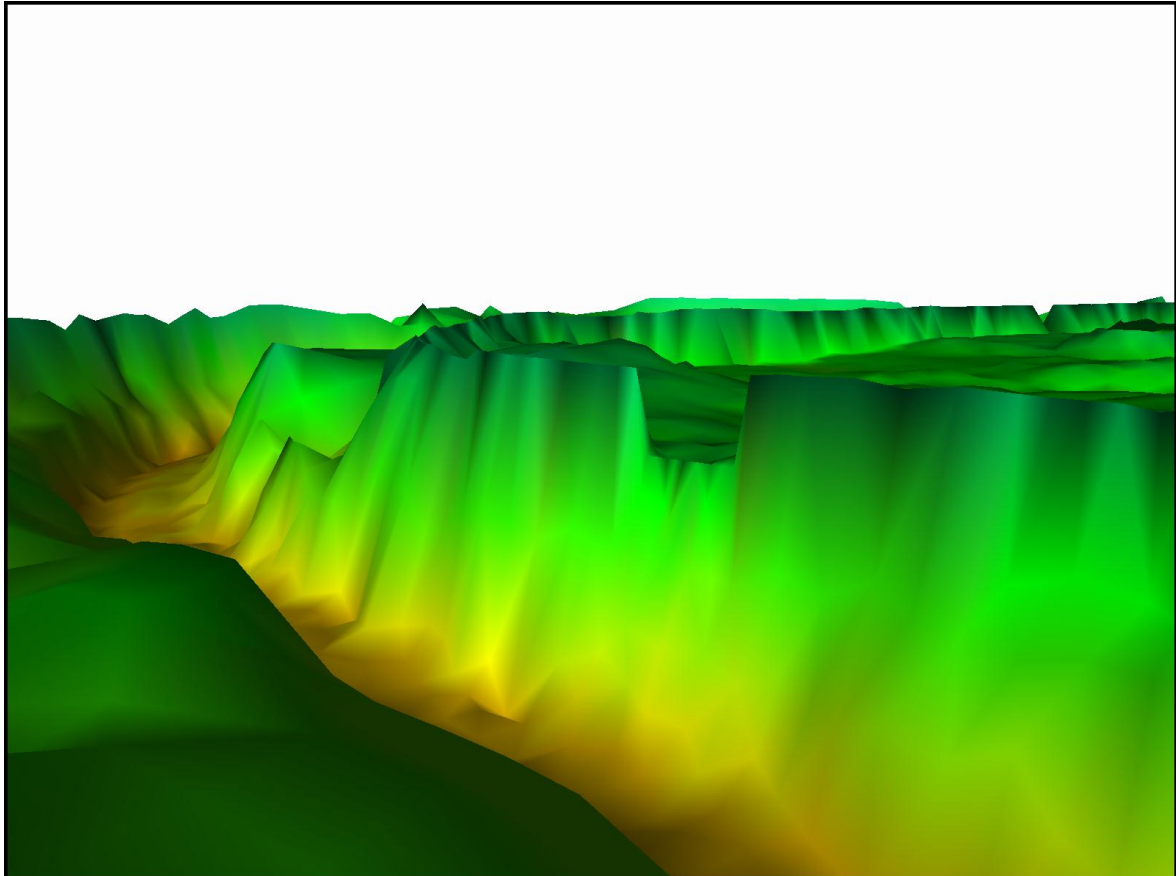


Figure 30: Created dike breach from a perspective of the opposite river bank

13.2 Results

Noticeable inflow at the breach location into the polder starts at the end of the 26th of January and peaks on the 29th of January at 1 pm with a flow rate of ca. 207 m³/s. Inflow continuous until the end of the 1st February, where the flow direction reverses to an outflow into the river (Figure 31).

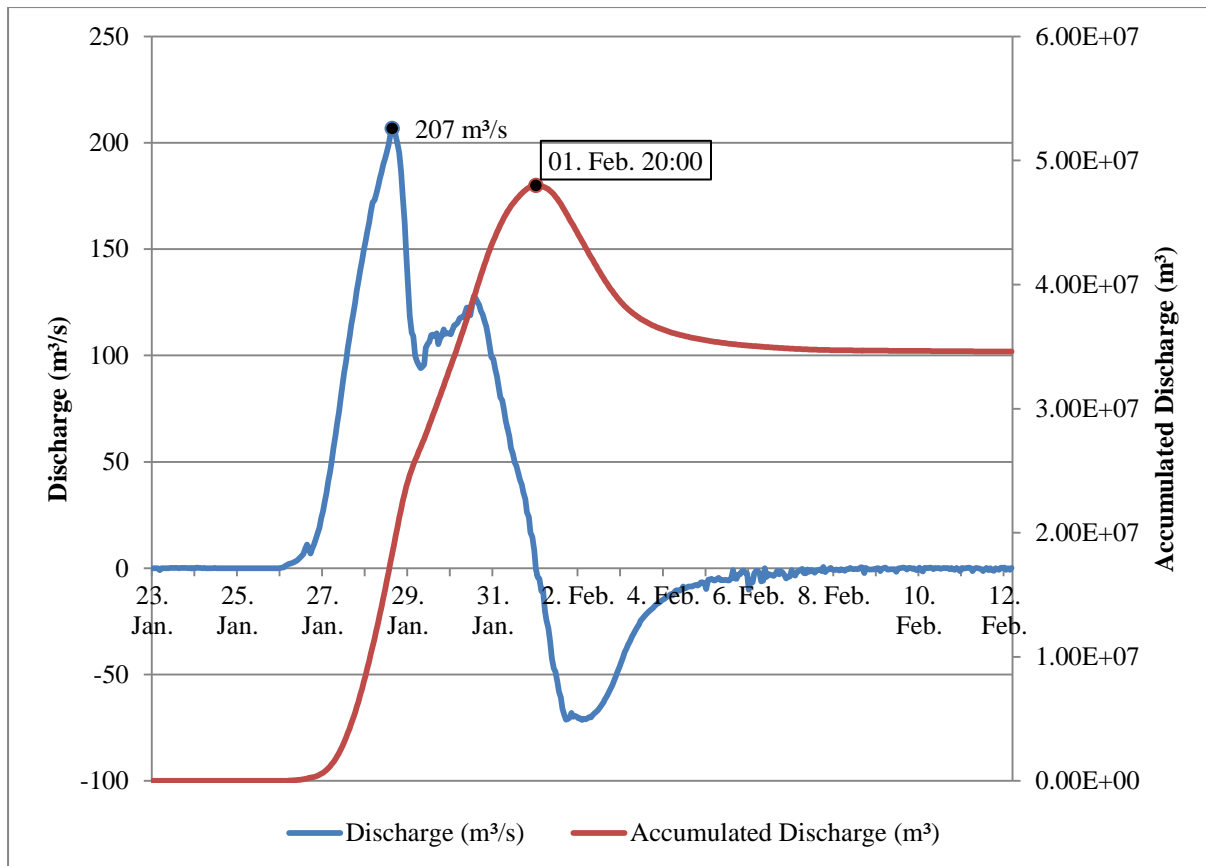
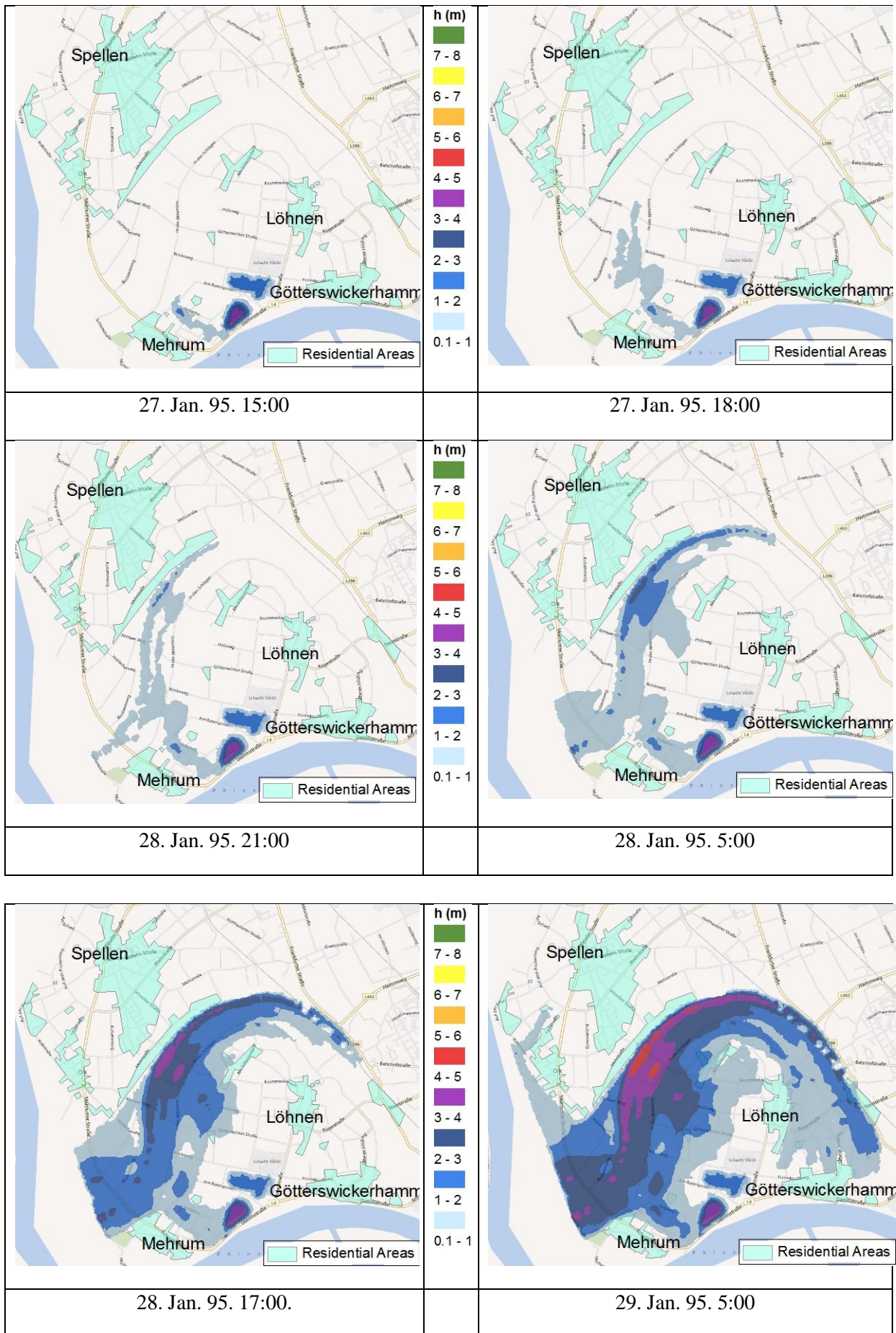


Figure 31: Dike breach induced inflow (instantaneous and accumulated) into the polder

14. Visualization of the Results in ArcGIS

Results of the simulation were visualized and analyzed within ArcGIS. Integrating flood inundation information obtained from NHMs into GIS systems allows the overlay of additional digital information. Thereby, affected buildings, roads and other facilities can be identified and the potential flood damage can be assessed.

The temporal development of the flood propagation within the polder was visualized in ArcGIS by creating TINs of the water depth for different time steps. For this, water depths of the center of each element within the polder were exported from an area time series at characteristic time steps as ASCII files. These files were then converted into point feature classes from which subsequently TINs were created. Each TIN was clipped to the relevant extend by using a polygon of the polder domain. Areas of zero water depth were removed from the visualization by specifying them as completely transparent. Furthermore, polygons surrounding the major residential areas were created by delineating them on a satellite image provided by Bing Maps Aerial. In this way, populated areas at risk can be identified, and the corresponding flood timing and water depth can be determined.



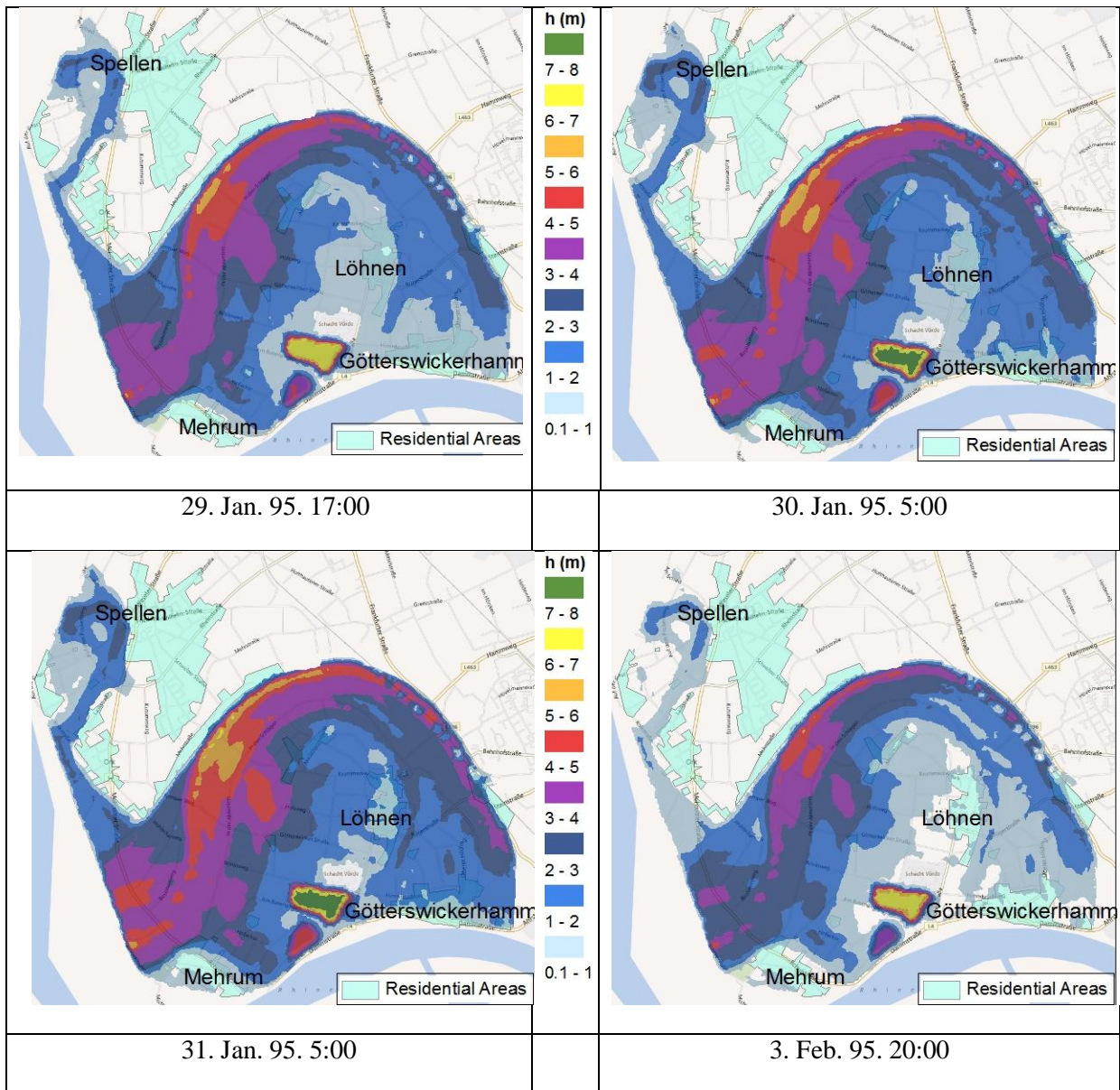


Figure 32: Temporal development of the inundation: Water depth within the polder at different time steps on a road map together with polygons for residential areas (Source: Bing Maps, 2012)

14.2 Discussion

Relatively large water depths were observed for large parts of the polder area. It has to be considered that the assumed complete dike failure for a stretch of 150 m already at an early phase of the flood event is a rather unlikely scenario. Certainly, the relatively slow development of the flood during the first four days would leave time to react and to prevent the intensity of the inundation to some degree. Furthermore, it has also to be considered that water flow is constrained to the defined boundaries which might in reality not be the case. Water depths are exaggerated also due to the neglect of infiltration processes. This particularly decreases the reliability of the model in predicting the recession of the flood and the duration of the inundation. Since the hazard associated to a flood event is besides the

inundation depth also considerably influenced by the destructive force of the water, a more thorough risk assessment would require to include flow velocities. These could be visualized in a similar way as was done for the water depth. The Flood Hazard Rating (HR) can be computed with the following formula:

$$HR = D \times (v + 0.5) + DF$$

where v is the velocity, D is the water depth and DF is a debris factor which ranges between 0 and 1, and indicates the probability that debris will result in a significantly greater damage (Evans et. al 2007).

15. Conclusion

The thesis presented the development of a 2-D river inundation model for a section of the Lower Rhine and the polder Mehrum using the software Mike 21 Flow Model fm. ArcGIS was applied for pre- and post-processing of the topographic data and the simulation results respectively. GIS-systems were found to be a valuable tool for facilitating and improving the creation of computational grids for NHMs. They particularly allow for a precise evaluation of the spatial coverage of available topographic data, and for an accurate determination of important hydraulic features such as dikes and the river banks. Furthermore, different sampling methods enable the modeler to extract a suitable volume of topographic data from a DEM according to the requirements of the case study. Especially, the tool “decimate TIN nodes” provides a good method for determining a set of nodes for a known maximum deviation of z-values from the original data. It was shown that local mesh refinements in important areas of the domain, the insertion of breaklines and the addition of nodes at topographically significant points can improve the performance of a NHM. The Mike Zero Animator tool allows visualizing created meshes in 3-D and can therefore be used to easily detect erroneous topographic representations within the model. Furthermore, it was concluded that the identification of a suitable roughness coefficient through calibration is an essential requirement for accurate predictions of the model. The creation of TINs from water depths outputs of Mike21fm was identified as a suitable method for displaying the inundation process within the polder. By superimposing these TINs onto different maps, affected areas and buildings can be identified and their vulnerability can be assessed. With this approach a detailed investigation of the flood risk in time and space could be conducted. Flood arrival times, water depths as well as extend and duration of the inundation can be obtained for

specific areas. On the basis of such flood maps, decision makers can be assisted in the development of flood risk management strategies, and the local population can be made aware of potential risks of a dike failures. These maps may also be useful for insurance and real estate companies for assessing potential economic damages. Flood risk management strategies could include evacuation plans, early warning systems, further structural measures to reduce the risk of inundation (e.g. secondary dikes) as well as restrictions on the development in particularly vulnerable areas.

16. Possible Future Steps

The river model could be potentially further improved by using a mesh which includes both triangular – and quadrangular elements, where the first would be used for the floodplains and the latter for the main channel. This approach is suggested by DHI for the modeling of rivers as it allows aligning the mesh in the direction of the flow. Moreover, for the quadrangular mesh M21fm offers a modified version of the inverse distance method which allows prioritizing data points located along the stream direction. Thereby, interpolation across the channel can be avoided which is a common problem for strongly meandering rivers when applying usual interpolation routines (Mandlbürger 2009).

For a more realistic representation of the dike breach, it would be necessary to account for the usually gradual development of such structural failures. One way this could be done without using a separate model for the breach would be to specify the breach location with an inflow which accounts for the temporal development of the dike failure. M21fm does not allow for the use of internal boundaries, and therefore the model would have to be downscaled to the size of the polder where then an open boundary could be specified with a time series of discharge values. These values could be derived from developed breach formulas which are given e.g. by Kamrath et al. 2006.

17. References

- Banic, J., and Cunningham, G. 1999. "Airborne Laser Bathymetry A Tool for the Next Millennium". Optech Inc. <http://www.docstoc.com/docs/55814093/Airborne-Laser-Bathymetry-A-Tool-for-the-Next-Millennium>.
- Bates, P.D, and De Roo, A.P.J. 2000. "A Simple Raster-based Model for Flood Inundation Simulation." *Journal of Hydrology* 236 (1–2) (September 10): 54–77.
doi:10.1016/S0022-1694(00)00278-X.
- BFG, 2012. . Undine. <http://undine.bafg.de>.
- Blazek, J. 2001. *Computational Fluid Dynamics: Principles and Applications*. Academic Pr Inc.
- Chua, L., Merting, F. and Holz, K. P. 2001. "River Inundation Modelling for Risk Analysis." In 1st International Conference on River Basin Management, Edited by: Falconer, RA and Blain, W. R, 373–382.
- Chung, T. J. 2002. *Computational Fluid Dynamics*. illustrated ed. Cambridge University Press.
- Cook, A., and Merwade, V. 2009. "Effect of Topographic Data, Geometric Configuration and Modeling Approach on Flood Inundation Mapping." *Journal of Hydrology* 377 (1–2) (October 20): 131–142. doi:10.1016/j.jhydrol.2009.08.015.
- Randall, D. 2006. "The Shallow Water Equations". Department of Atmospheric Science Colorado state University.
- DHI. 2007. "Mike 21 & Mike 3 Flow Mode FM: Hydrodynamic and Transport Module. Scientific Documentation." Danish Hydraulic Institute. 2007b. "Mike 21 Flow Model: Hints and Recommendations in Applications with Significant Flooding and Drying". Danish Hydraulic Institute. 2009. "Mike Zero: Creating 2D Bathymetries. Bathymetry Editor & Mesh Generation. Scientific Document". Danish Hydraulic Institute.
- DHI. 2011. "Mike 21 Flow Model: Hydrodynamic Module User Guide". Danish Hydraulic Institute.
- ESRI. 2012. "ArcGIS Help Library: Arcgis 10."
- Evans, S. Y, Gunn, N. and Williams, D. 2007. "Use of GIS in Flood Risk Mapping." In National Hydrology Seminar GIS (Geographic Information Systems) in Hydrology Applications-Modelling-Data Issues, 1–12.
<http://citeseerx.ist.psu.edu/viewdoc/download?doi=10.1.1.133.7813&rep=rep1&type=pdf>.

- Fisher, K., and Dawson H. 2003. "Reducing Uncertainty in River Flood Conveyance: Roughness Review". DEFRA/Environment Agency: Flood and Coastal Defence R&D Programme. www.river-conveyance.net/ces/documents/RoughnessReviewFinal_July07.pdf.
- Green, I. R., and Stephenson A.. 1986. "Criteria for Comparison of Single Event Models." *Hydrological Sciences Journal* 31 (3): 395–411. doi:10.1080/02626668609491056.
- Habersack, H., Hengl, M., Knoblauch, H. and Tritthart M. 2007. "Fließgewässermodellierung - Arbeitsbehelf Hydrodynamik Grundlagen, Anwendung Und Modelle Für Die Praxis". Bundesministerium für Land- und Forstwirtschaft, Umwelt und Wasserwirtschaft. Österreichischer Wasser- und Abfallwirtschaftsverband (ÖWAV).
- Horritt, M.S, and Bates, P.D. 2001. "Effects of Spatial Resolution on a Raster Based Model of Flood Flow." *Journal of Hydrology* 253 (1–4) (November 15): 239–249. doi:10.1016/S0022-1694(01)00490-5.
- Horritt, M.S., and Bates, P.D.. 2002. "Evaluation of 1D and 2D Numerical Models for Predicting River Flood Inundation." *Journal of Hydrology* 268 (1–4) (November 1): 87–99. doi:10.1016/S0022-1694(02)00121-X.
- Horritt, M.S., Bates, P.D. and Mattinson M.J. 2006. "Effects of Mesh Resolution and Topographic Representation in 2D Finite Volume Models of Shallow Water Fluvial Flow." *Journal of Hydrology* 329 (1–2) (September 30): 306–314. doi:10.1016/j.jhydrol.2006.02.016.
- Kamrath, P., Disse M., Hammer, M. and Köngeter J. 2006. "Assessment of Discharge Through a Dike Breach and Simulation of Flood Wave Propagation." *Natural Hazards* 38 (1): 63–78. doi:10.1007/s11069-005-8600-x.
- Koppe, W. 2012. Klett. Infoblatt Rhine: Rhine -Verlauf, Ausbau, Ökologie. http://www2.klett.de/sixcms/list.php?page=infothek_artikel&extra=TERRA-Online%20/%20Gymnasium&artikel_id=108943&inhalt=klett71prod_1.c.136783.de.
- Krause, P., Boyle, D. P. Bäse, F. and others. 2005. "Comparison of Different Efficiency Criteria for Hydrological Model Assessment." *Advances in Geosciences* 5: 89–97.
- Malcherek, A. 2012. "Fließgewässer: Hydromechanik Und Wasserbau. Version 3.0." Institut für Wasserwesen. <http://dokumente.unibw.de/pub/bscw.cgi/d1831313/Skript%203%20-%20Flie%C3%9Fgew%C3%A4sser.pdf>.

- Mandlbürger, G. 2009. *Topographische Modelle Für Anwendungen in Hydraulik Und Hydrologie: Aufbau Und Aufbereitung Digitaler Wasserlauf-Geländemodelle*. Südwestdeutscher Verlag für Hochschulschriften.
- Merwade, V., Cook, A. and Coonrod, J.. 2008. “GIS Techniques for Creating River Terrain Models for Hydrodynamic Modeling and Flood Inundation Mapping.” *Environmental Modelling & Software* 23 (10–11) (October): 1300–1311. doi:10.1016/j.envsoft.2008.03.005.
- Pappenberger, F., Patrick M., Keith J. B., Henry J.-B., Pfister, L. and Fraipont, P. 2006. “Influence of Uncertain Boundary Conditions and Model Structure on Flood Inundation Predictions.” *Advances in Water Resources* 29 (10) (October): 1430–1449. doi:10.1016/j.advwatres.2005.11.012.
- Reutebuch, S. E. R., McGaughey, J., Andersen H. E., and Carson, W. 2003. “Accuracy of a High-resolution Lidar Terrain Model Under a Conifer Forest Canopy.” <http://ddr.nal.usda.gov/handle/10113/47657>.
- Schumann, G., Matgen, P., Hoffmann, L., Hostache, R., Pappenberger, F. and Pfister, L.. 2007. “Deriving Distributed Roughness Values from Satellite Radar Data for Flood Inundation Modelling.” *Journal of Hydrology* 344 (1–2) (September 30): 96–111. doi:10.1016/j.jhydrol.2007.06.024.
- Shewchuk, J. 1996. “Triangle: Engineering a 2D Quality Mesh Generator and Delaunay Triangulator.” *Applied Computational Geometry Towards Geometric Engineering*: 203–222.
- Straatsma, M., and Huthoff, F. 2011. “Uncertainty in 2D Hydrodynamic Models from Errors in Roughness Parameterization Based on Aerial Images.” *Physics and Chemistry of the Earth, Parts A/B/C* 36 (7–8): 324–334. doi:10.1016/j.pce.2011.02.009.
- Thu, P. T.M., Goebel, N., and Nestmann, F. 2002. “A Hydrodynamic-numerical Model of the River Rhine.” <http://library.witpress.com/pages/PaperInfo.asp?PaperID=454>.
- Vivoni, E. R, Ivanov, V. Y., Bras, R. L. and Entekhabi, V. 2004. “Generation of Triangulated Irregular Networks Based on Hydrological Similarity.” *Journal of Hydrologic Engineering* 9: 288.
- Vorogushyn, S. 2008. “Analysis of Flood Hazard Under Consideration of Dike Breaches”. *Universitätsbibliothek*. <http://opus.kobv.de/ubp/volltexte/2009/2764/>.
- Weih Jr, R. C. 2010. “Assessing the Vertical Accuracy of Arkansas Five-Meter Digital Elevation Model for Different Physiographic Regions.” *Journal of the Arkansas Academy of Science* 64: 123.

- Willmott, C. J, and Matsuura, K. 2005. “Advantages of the Mean Absolute Error (MAE) over the Root Mean Square Error (RMSE) in Assessing Average Model Performance.” *Climate Research* 30 (1): 79.
- Wright, N., and Crosato, A. 2011. “2.07 - The Hydrodynamics and Morphodynamics of Rivers.” In *Treatise on Water Science*, 135–156. Oxford: Elsevier.
<http://www.sciencedirect.com/science/article/pii/B9780444531995000336>.
- WSV. 2012. “Wasserstände an Schifffahrtsrelevanten Pegeln.” Wasser- Und Schifffahrtsverwaltung Des Bundes: Elektronischer Wasserstraßen-Informationsservice (ELWIS).
http://www.elwis.de/gewaesserkunde/Wasserstaende/Wasserstaende_start.php?target=2&gw=RHINE.
- Zhang, M., and Wu, W.M. 2011. “ Two Dimensional Hydrodynamic and Sediment Transport Model for Dam Break Based on Finite Volume Method with Quadtree Grid.” *Applied Ocean Research* 33 (4) (October): 297–308. doi:10.1016/j.apor.2011.07.004.

Appendix:

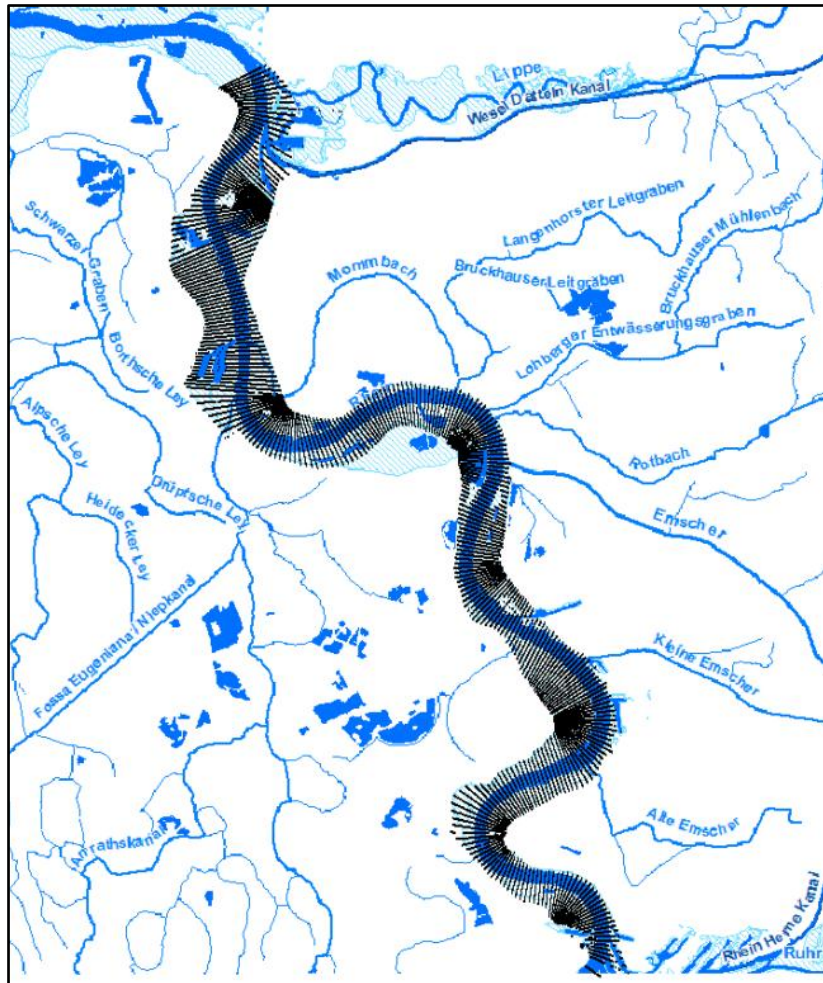


Figure 33: Available topographic data on a river map (Source: Geoserver NRW, 2012)

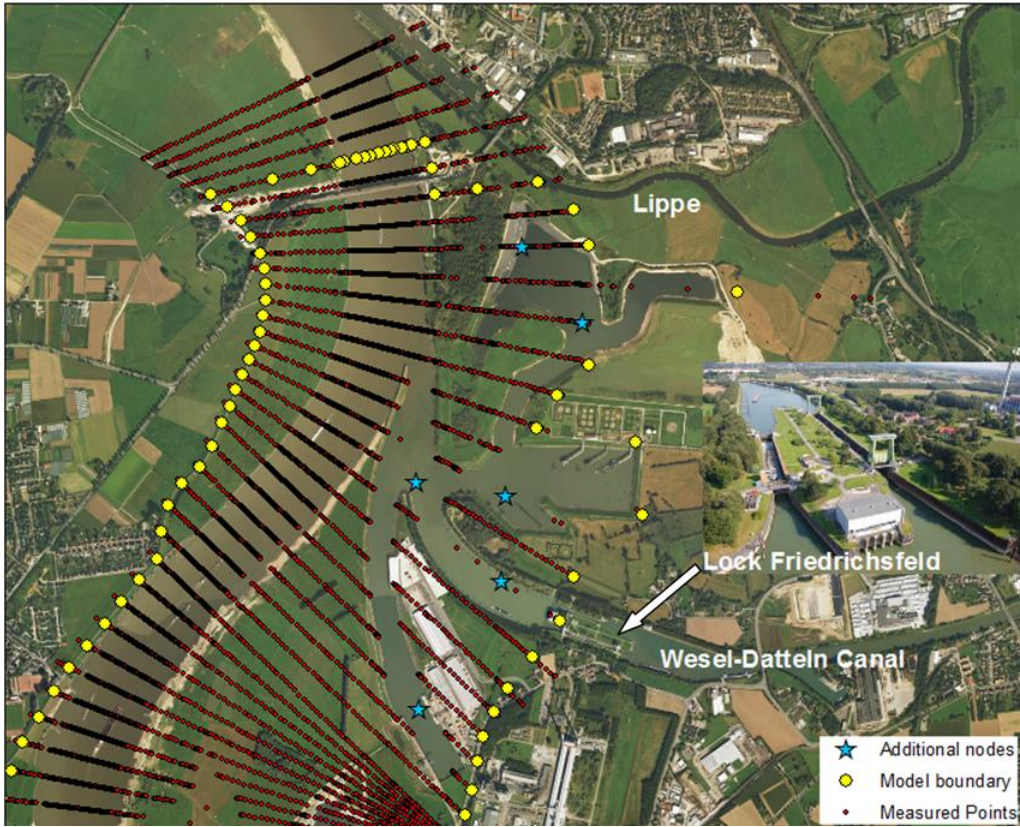


Figure 34: Model boundary at the upper section of the river (Source: Bing Maps Aerial, 2012)

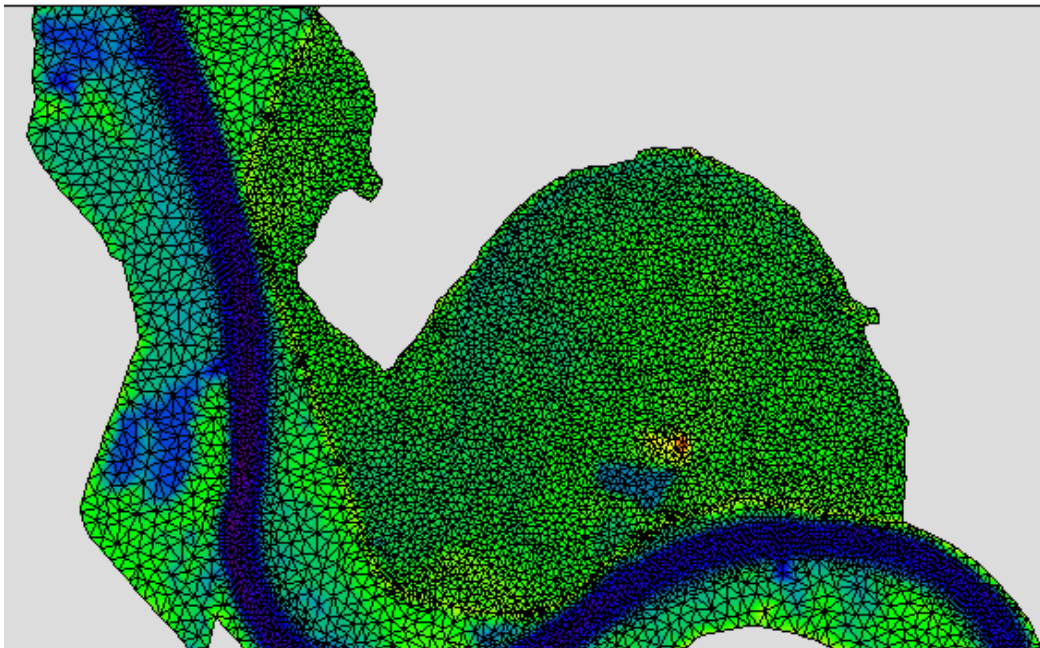


Figure 35: Mesh of the polder and the river channel



Figure 36: Boundary along the dike separating the polder Mehrum from the river

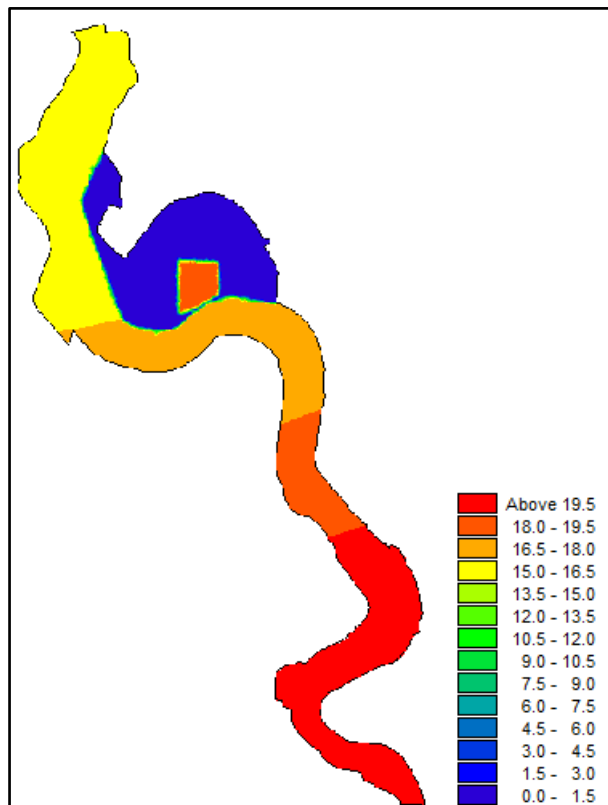


Figure 37: Initial Conditions

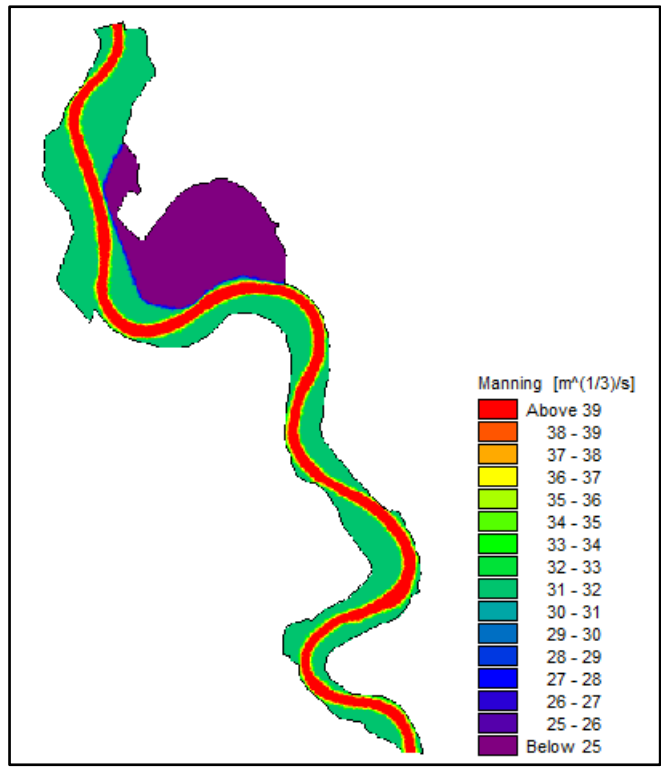


Figure 38: Specified Manning values

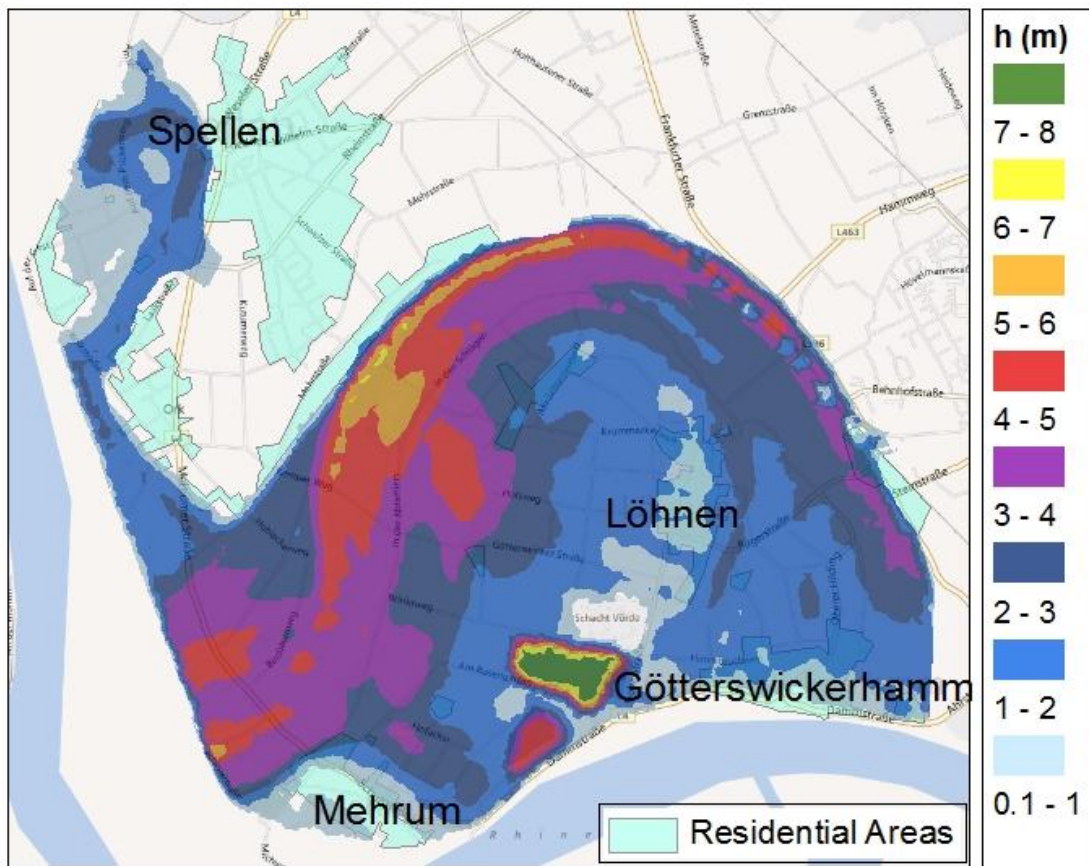


Figure 39: Maximum inundation of the polder

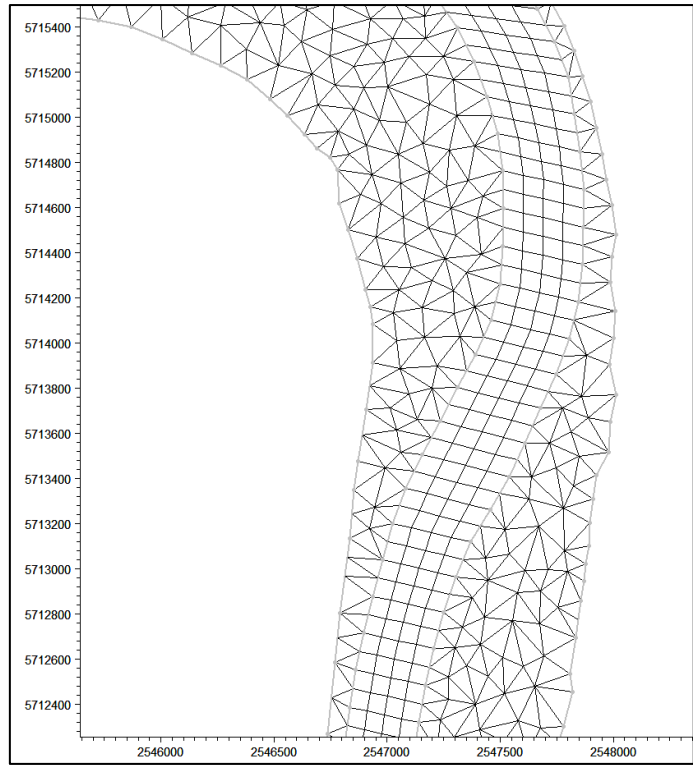


Figure 40: Mesh containing quadrangular elements for the main channel